NANOCATALYSIS USING PLASMONIC NANOPARTICLES

M.Sc. Thesis

By

SHARMA PUNIT BIJENDRA

DEPARTMENT OF CHEMISTRY
INDIAN INSTITUTE OF TECHNOLOGY INDORE

MAY, 2020

NANOCATALYSIS USING PLASMONIC NANOPARTICLES

A THESIS

Submitted in partial fulfillment of the
requirements for the award of the degree
of
Master of Science

by
SHARMA PUNIT BIJENDRA

DEPARTMENT OF CHEMISTRY
INDIAN INSTITUTE OF TECHNOLOGY INDORE

MAY, 2020

INDIAN INSTITUTE OF TECHNOLOGY INDORE

CANDIDATE'S DECLARATION

I hereby certify that the work which is being presented in the thesis entitled **NANOCATALYSIS USING PLASMONIC NANOPARTICLES** in the partial fulfillment of the requirements for the award of the degree of **MASTER OF SCIENCE** and submitted to the **DEPARTMENT OF CHEMISTRY, Indian Institute of Technology Indore**, is an authentic record of my own work carried out during the time period from August 2021 to June 2022 under the supervision of Dr. Tridib Kumar Sarma Associate professor, Department of Chemistry, IIT Indore.

The matter presented in this thesis has not been submitted by me for the award of any other degree of this or any other institute.

Punit 27/05/2022

Signature of the student with date
(SHARMA PUNIT BIJENDRA)

This is to certify that the above statement made by the candidate is correct to the best of my knowledge.

Tridib K. Sarma 27/05/2022

Signature of the Supervisor (with date)
(Dr. Tridib Kumar Sarma)

SHARMA PUNIT BIJENDRA has successfully given his M.Sc. Oral Examination held on **24/05/2022.**

Tridib K. Sarma

Signature(s) of Supervisor(s) of MSc thesis
Date: 27/05/2022

Tushar kanti Mukherjee

Convener, DPGC
Date: 27/05/2022

Signature of PSPC Member 1
Date: 27/05/2022

Tushar kanti Mukherjee

Signature of PSPC Member 2
Date: 27/05/2022

-

ACKNOWLEDGEMENTS

This thesis is the end of my trip to the master's degree. This thesis has been revised on how to complement the support and encouragement of many people including my friends, colleagues, and various institutions. At the end of my thesis, it is a pleasant task to express my thanks to all those who have contributed in many ways to the success of this study and made it an unforgettable experience for me. First and foremost, I wish to thank my supervisor, Dr. Tridib Kumar Sarma. He has been very supportive since the days I began working in his lab. His knowledge, valuable advice, constant motivation, affectionate attitude, understanding, patience, and good criticism have greatly improved my experience. Without his continuous inspiration, this study could not be completed.

I owe my special thanks to my PSPC committee members Dr. Tushar K. Mukherjee, Dr. Satya S. Bulusu and DPGC convener Dr. Tushar K. Mukherjee for their valuable ideas and guidance. I am highly thankful to Prof. Biswarup Pathak, Head, Department of Chemistry for their valuable suggestions that have been very helpful for this study. I would also like to thank all the Faculty, Department of chemistry, IIT Indore for their humble and supportive gesture. Also, I would like to thank SIC IIT Indore for providing the characterization facilities.

I immensely extend my thanks to Ms. Vidhi Agarwal and Ms. Amrita Chakraborty who helped me during my whole project. I also extend my thanks to my group members Mr. Tarun Sahu, Mr. Surya K. Sarma, Mr. Aditya Prasun, Mr. Ravindra Vishwakarma for their consistent support, broadening transparency and broadening horizons during my project. I sincerely extend my thanks to all my classmates and I feel a deep sense of gratitude to my family for their unconditional love and support during this tenure.

SHARMA PUNIT BIJENDRA

LIST OF SYMBOLS OR ABBREVIATIONS

NPs	Nanoparticles	H_2	Hydrogen
nm	Nanometer	CH_4	Methane
mg	milligram	C_2H_5OH	Ethanol
mL	milliliter	CH_3OH	Methanol
mM	millimolar	Ag	Silver
VB	Valence band	CDs	Carbon dots
SPR	Surface plasmon resonance	PL	Photoluminescence
PVP	Polyvinyl pyrrolidone	$AgNO_3$	Silver nitrate
PEI	Polyethyleneimine	$NaBH_4$	Sodium borohydride
UV	Ultraviolet	L-Cys	L-Cysteine
DI	Deionized	CA	Citric acid
FE-SEM	Field emission scanning electron microscope	K_2CO_3	Potassium carbonate
FT-IR	Fourier transform infrared spectroscopy	mV	millivolt
PXRD	Powder X-ray diffraction	H_2O	water
TBHP	Tert-Butyl hydroperoxide	CH_3CN	Acetonitrile

LIST OF FIGURES

TABLE OF CONTENTS

A. INTRODUCTION

Nanotechnology is a growing branch of science that focuses on the design, production, and manipulation of particle formation with sizes ranging from 1 to 100 nanometer. Due to their small dimensions, the nanoparticles demonstrate completely different physico-chemical and surface properties compared to their bulk counterparts. Nanoparticles (NPs) have tremendous application potential in a variety of fields, including health care, food, mechanics, optics, environmental health, biomedical sciences, cosmetics, chemical industries, electronics, space industries, drug-gene delivery, energy science and so on. It is an interdisciplinary approach that includes biology, chemistry, biochemistry, physics, medicine, and engineering, as well as the exploratory use of NPs in biological systems. Furthermore, nanotechnology is a critical approach in the creation of clean, nontoxic, and environmentally acceptable techniques for the synthesis and assembly of metal NPs with the inherent potential to reduce metals via certain metabolic pathways.

Nowadays, there is a rising demand to design environmentally-friendly synthesis techniques that do not involve harmful compounds. Use of native biomolecules such as polysaccharides, proteins and nucleobases along with techniques such as use of visible light irradiation are examples of green synthesis approaches that have benefits over traditional methods that use chemical agents which are detrimental to the environment. The most essential aspects to address in green NP synthesis are solvent medium selection and use of eco-friendly nontoxic reducing and stabilising agent.

One of the primary research areas dedicated to addressing the obstacles on this path is sustainable chemistry. Catalysis is critical for sustainable chemistry; catalysts can enhance process economy while lowering net greenhouse gas emissions and waste volume. Green chemistry techniques, notably in the synthesis of contemporary catalysts and in analysis practises, need to incorporate more sustainability considerations. Catalysis has matured into a well-defined study field with well-defined ideas and concepts.

Today, researchers in the field of catalysis are looking for new catalysts to enhance the performance of existing catalysts or to design catalysts for new processes. Catalysts showing great activity, efficiency, stability, and selectivity all at the same time are the top performers. The energy, electrical, optical, and photonic efficiencies are all taken into account while evaluating their performance. Putting this understanding into practise allows researchers to create custom catalysts, such as materials with specific properties. Nanospheres, nanosheets, nanograins, nanoclusters, and nanofibers are only few of the morphologies that nanoparticles (NPs) can take. They are substances that have a cross-section of less than 100 nanometre and are shaped as any irregular shape. Composites, compounds, alloys, and elemental solids are some of the substances that can be used. Nano catalysts are a hybrid of homogeneous and heterogeneous catalysts, offering advantages in terms of activity, efficiency, selectivity, and reusability in many circumstances. They are able to go beyond the constraints of homogeneous and heterogeneous catalysts by utilising nano-effects. Nanopore confinement causes catalytic nano-effects due to its structural, quantum size, and electrical effects.

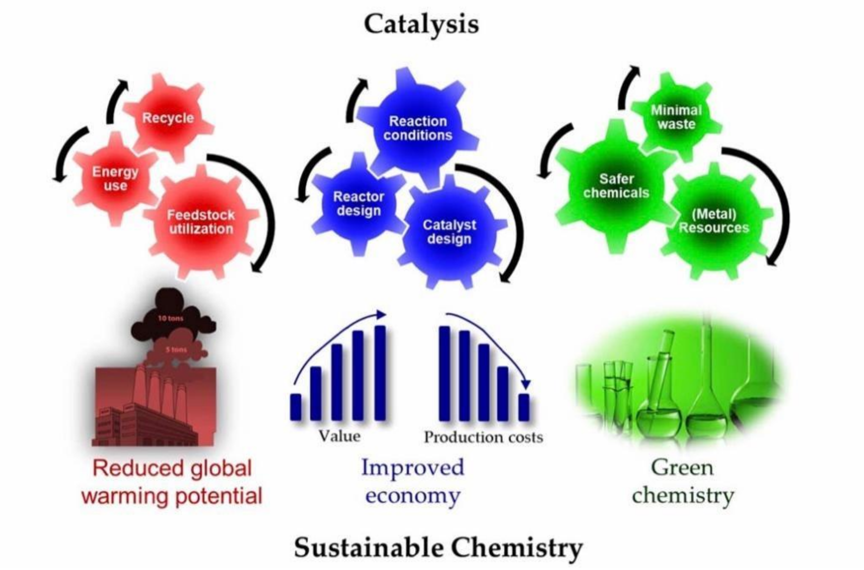

Fig.1. Utility of catalyst [1]

As shown in Figure 1 [1], the catalyst is a proponent in Sustainable Chemistry as it reduces global warming through its application to green chemistry.

Catalysis plays an essential role in green chemistry concepts because it minimises the cost of unit production, waste, and energy consumption related with chemical processes. Recent advances in petroleum refining employing Nano catalysts have been evaluated. Nano catalysts have also demonstrated enormous promise in the generation of bulk chemicals from renewable sources. Fine chemicals can also be made from biomass, in addition to petroleum. The generation of terpenes and their oxides is one such example (e.g., a-pinene oxide. Nano catalysts give chances to enhance energy efficiency and lower the carbon footprint of a process, to reduce waste quantities and enhancing process economics. Hydrogen (H_2) is regarded as one of the most environmentally friendly energy sources for the future. Currently, the great majority of industrial H_2 is produced by reforming reactions involving CH_4, C_2H_5OH, CH_3OH, acetic acid, and other hydrocarbons. These processes necessitate severe conditions, which include substantial energy consumption as well as strong catalytic deactivation effects. Photocatalytic H_2 synthesis uses significantly less energy, but results in significantly slower kinetics and lower yields. Various green production strategies for Nano catalysts have gained popularity in recent years. The usage and recycling of metals is another key sustainability element in terms of resource management. TMOs have been studied extensively as a noble metal alternative. To investigate transition metal catalysts, many models which use the Sabatier principle, activity maps, d-band energy, coordination number, and Slater orbitals have been utilised, with computational chemistry playing a key role. Carbon-derived nanomaterials are intriguing metal-free options that have the potential to replace Pt catalysts in a variety of organic transformations, not just electrocatalysis (e.g., hydrogenations).

The thermodynamics of photocatalysis and catalysis are the most significant distinction. In a broad sense, a catalyst lowers the activation energy (E_a) of a chemical process by altering intermediate states, hence speeding up a reaction that occurs spontaneously with negative value of Gibbs free energy change, i.e., catalysis is restricted to thermodynamically possible reactions as shown in Figure 2[15]. Photocatalysis, on the other hand, is widely known for driving energy-storing processes, such as splitting water into H_2 and O_2.

In this regard, "photocatalysis" must be distinguished from "catalysis" as a distinct term.In fact, when compared to catalytic reactions, the apparent activation energy (E_a) of photo catalysis calculated using an Arrhenius plot has been detected to be relatively low. A schematic description of the electronic structures of semiconducting materials, known as a band model, is frequently used to explain the theory of photocatalysis. Photoirradiation excites an electron in an electron-filled valence band to an empty conduction band, which is separated from the VB by a forbidden band, or band gap, leaving a positive hole in the valence band. These electrons and positive holes promote the reduction and oxidation of substances adsorbed on a photocatalyst's surface, respectively. This way is used to examine the photocatalytic reactions of semiconducting and insulating materials. However, no such limitation based on the electrical structure of a photocatalyst is included in the above-mentioned definition of "photocatalysis." For example, a photocatalyst can be an isolated chemical species on or in a solid that does not have the above-mentioned band structure, and even when a bulk material is used, the photo-absorption and subsequent photocatalytic reaction can occur at a localised site when photocatalysts are photo irradiated at a wavelength nearby band gap. A gold-modified titania photocatalyst, for example, produces "photocatalytic" breakdown of organic molecules in aerated conditions by photo absorption of gold particles' surface-plasmon resonance (SPR). As a result, adopting a band model to interpret data is not always sufficient for understanding photocatalysis.

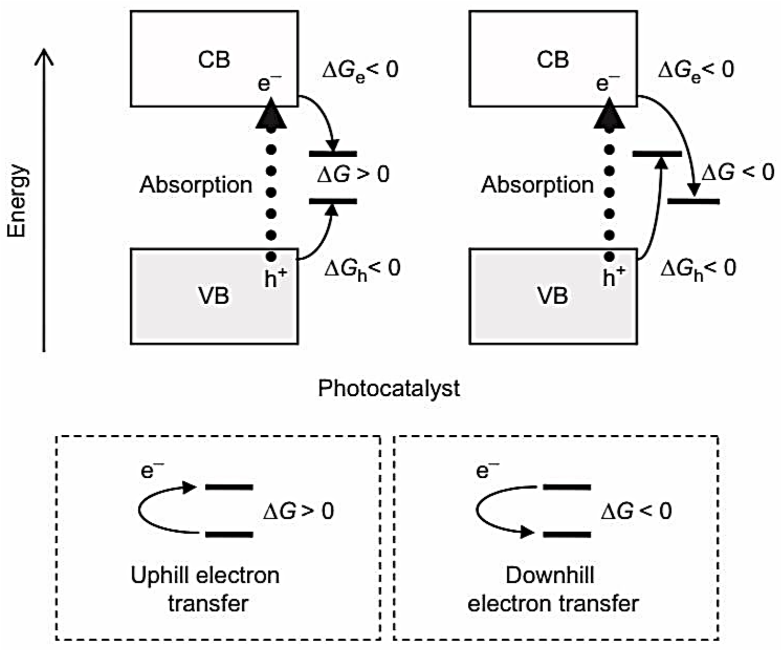

Fig.2. Gibbs-Free Energy change in photocatalytic reaction. [15]

M. C. Lea's ground-breaking study on the production of silver nanoparticles (Ag NPs) in 1889 piqued the scientific community's interest and signalled the start of a new era in nanoscience and nanotechnology. The size of Ag NPs typically ranges from 1 to 100 nanometres. The remarkable features of these nanometric-sized silver particles, as well as their adaptability, sparked modern-day innovation. Silver has three distinct properties: maximum electrical and thermal conductivity, as well as exceptional brightness. Nano silver not only has various applications in academia, but it also has a number of significant advantages in medical, agriculture, electronics, food industry, robotics, electronics, food industry, textile industry, and other fields. As a result, considerable work has gone into the design and synthesis of silver nanoparticles of various sizes and forms, such as rods, plates, wires, prisms, cubes, and tubes. Ag NPs come in a variety of forms and sizes, which affect their electromagnetic properties, optical, and chemical. Ag NPs have been synthesised using a variety of synthetic techniques and assemblies to suit a variety of purposes.

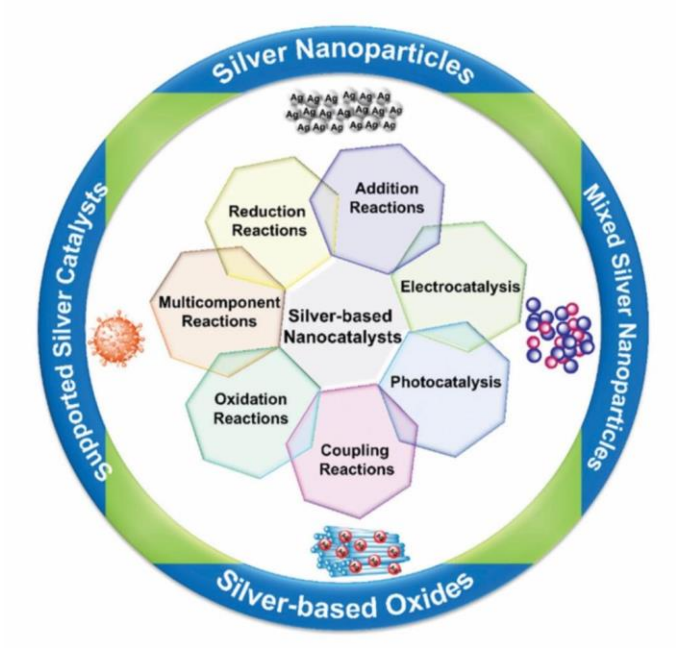

Fig.3. Applications of Ag-based Nanoparticles [2]

Furthermore, researchers have moved their focus to the preparation of more complex or hybrid silver-based nanomaterials, whose tuneable properties allow for noteworthy applications in technology-driven areas. It's worth noting that Ag NPs have aided in the improvement of catalytic processes in particular. The unique proliferation is because of these nano-sized particles do not only have a large surface area but they also contain a large fraction of coordinatively unsaturated atoms that enhance overall catalytic efficiency by coordinating with substrates. Ag NPs' superior antibacterial and localised surface plasmon resonance properties make them ideal for broad-spectrum antimicrobials, chemical/biological sensors and biomarkers, biomedical materials, surface-enhanced Raman spectroscopy (SERS), and other applications. The biological activity of Ag NPs is affected by shape, size distribution, surface chemistry, particle composition, particle morphology, coating/capping, particle reactivity in solution, agglomeration, dissolution rate, ion release efficiency, and the cell type involved. The type of reducing agents used in the synthesis of Ag NPs is a critical factor in determining cytotoxicity. These outstanding characteristics of Ag NPs have prompted scientists to develop potent catalysts that may be used in industrial operations as mentioned in Figure 3 [2].

In addition, the continual increase in the number of papers dedicated to Ag-based materials can be directly associated with the noteworthy advancement in this domain.

Carbon-based materials are crucial to the advancement of material science. These materials have got applications in many areas due to their environmental-friendly nature as shown in Figure 4. From conventional industrial carbon such as activated carbon, carbon black etc. to new industrial carbon like carbon fibres, graphite etc. and new carbon nanomaterials like graphene and carbon nanotubes, research and applications of carbon-based materials have always been popular in chemistry discipline, Macroscopic carbon material, on the other hand, lacks the necessary band gap, making it impossible to use as a luminous material. Due to their outstanding photoluminescence (PL), excellent quantum yield (QY), less toxicity, small size, appreciable biocompatibility, and abundant cheap sources, carbon dots (CDs), a new rising star in the carbon family, have received a lot of attention. They have important applications in the field of chemistry and medicine.

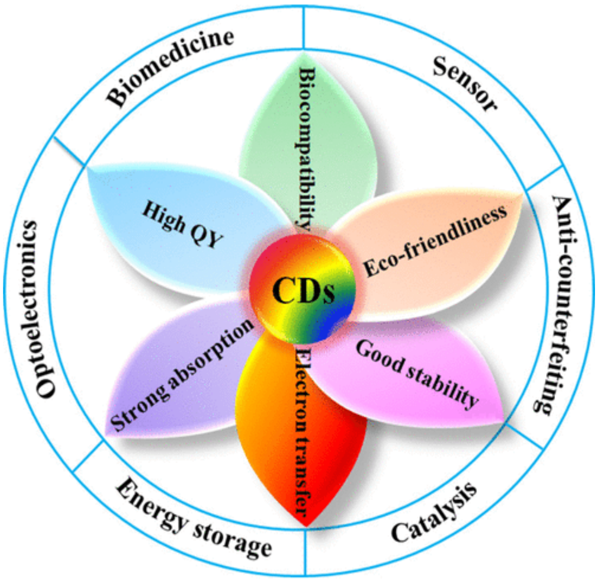

Fig.4. Applications of CDs [16]

Since their accidental discovery in 2004 while isolating and purifying single walled Carbon nanotubes, fluorescent carbon dots (CDs) have sparked worldwide interest. Many approaches, including hydrothermal treatment, thermal decomposition, ultrasonic-microwave irradiation and chemical oxidation have been employed to produce fluorescent CDs. However, most of these processes involve expensive energy-intensive equipment or significant quantities of toxic chemicals, making the CD production process complex and challenging. As a result, developing easy and ecologically friendly ways for making luminous CDs is critical. Natural biomass is abundant, sustainable, and renewable, inexpensive, and available on a large scale. CDs provide a number of advantages over typical semiconductor quantum dots and organic fluorescent dyes, including photo-stability, no bleaching or blinking fluorescence, and excitation-dependent emission fluorescence. Fluorescent CDs are also chemically stable, have strong water solubility, are low in cytotoxicity, and have a high biocompatibility. CDs are mainly used in fluorescence imaging, fluorescence detection, drug delivery, and catalysis due to their versatile features. Fluorescent CDs are currently employed to stabilize and reduce metal nanomaterials, which were regarded to be an outstanding electron acceptor and electron donor; on account of their abundant oxygen-containing functional groups such as hydroxyl, carbonyl, carboxyl, and epoxy on their surface. Fluorescent CDs, in particular, were chosen as a reducing and stabilizing agent that can be employed to produce silver nanoparticles (AgNPs) with enhanced antibacterial properties. Silver nanoparticles, in particular, have been widely used in a variety of bactericidal applications against a variety of bacteria and viruses. Silver nanoparticles have a stronger bactericidal ability and a lower cost than most other antibacterial materials, such as quaternary ammonium compounds, metal ions, and medicines, and they can gently release silver ions to inactivate germs. CDs can act as reducing agent for the reduction of silver ions and the stabilization of nanoparticles, and the addition of fluorescent CDs to Ag nanoparticles enhances the negative surface charge and hydrophilicity. Meanwhile, due to their close proximity, silver nanoparticles might quench fluorescent CDs, resulting in surface plasmon increased energy transfer from CDs to AgNPs.

Although a lot of work has gone into developing the CDs/AgNPs composite, reducing agents such as Citric acid, sodium citrate, and sodium borohydride are still employed to help reduce silver ions. As a result, the procedure is complicated and toxic, hence obtaining CDs/AgNPs composites using a simple and environmentally safe method is preferable.

Since, the last few decades photocatalysis become a prominent field of research due to its green and sustainable aspects. With keeping these characteristics in mind, we tried to develop the carbon dot composite Ag NPs. Since carbon dot itself is a efficient photocatalyst so, the question arises why are we trying to develop Nanocomposite. This we may try to understand through its optical properties. When a light is incident, the electrons get excited and move to conduction band thereby generating the positive holes in the valence band. But in the case of carbon dots, these electrons recombined with the positive holes due to the electrostatic force of attraction, resulting in a decreased in catalytic efficiency. Thus, we are introducing a metal ion which contain electrons on its surface which repel with the excitons and maintain the separation between the excitons and the holes. This results in the enhancement of catalytic efficiency. Hence in this work, we have successfully synthesised the Ag nanocomposites under the various conditions and also characterised through various techniques. We may infer that our synthesised Ag nanocomposite might work as a potential photocatalyst as it is absorbing light in the visible region.

B. SYNTHETIC SCHEMES

I. Sodium citrate capped silver nanoparticles

Silver nanoparticles were produced in aqueous solution by reducing silver nitrate with sodium borohydride and stabilising them with sodium citrate. Analytical grade reagents were employed throughout the synthesis. In an ice/water bath at roughly 0C, 5 mM of a 5 ml aqueous silver nitrate solution was added to 1.06 mM of a 16 ml aqueous sodium citrate solution under magnetic stirring. Then, over the course of 5 minutes, 100 uL of a freshly produced 100 mM aqueous sodium borohydride solution was added dropwise in the above solution. The initially colourless solution turned yellow after being agitated for 1 hour and 45 minutes at roughly 0°C. As illustrated in fig.5, yellow coloured Ag NPs were obtained.[4]

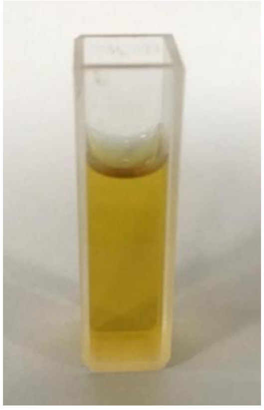

Fig.5. Citrate capped Ag nanoparticle

II. Polyvinyl pyrrolidone (PVP) capped silver nanoparticles

Silver nanoparticles were produced in aqueous solution by reducing silver nitrate with sodium borohydride and stabilising them with polyvinyl pyrrolidone. 4.2 mg $AgNO_3$ in 5 mL water, 4.3 mg PVP in 16 mL water, and 3.9 mg $NaBH_4$ in 1 mL water were first made. In an ice/water bath at roughly 0°C, 1 mL of prepared aqueous silver nitrate solution; then added to 16 mL of prepared aqueous PVP solution under magnetic stirring. Then, over the course of 5 minutes, 100 uL of a freshly produced 100 mM aqueous sodium borohydride solution was added dropwise. The prepared colourless solution turned yellow after being agitated for 1 hour and 45 minutes at roughly 0°C. As illustrated in fig.6, yellow coloured Ag NPs were obtained.[5]

Fig.6. PVP capped Ag nanoparticle

III. Silver doped carbon dot

75 mg polyethyleneimine (PEI) and 100 mg $AgNO_3$ were dissolved in 2.5 mL DI water and agitated for 1 hour at room temperature. To make the solution 12.5 mL, 125 mg citric acid was added to the aforesaid solution, along with DI water. The solution was then transferred to a stainless-steel autoclave with a Teflon lining, which was subsequently baked for four hours at 200°C. The solution of CD was light yellow in daylight, and exhibited blue fluorescence under UV light, as shown in fig.7 & 8. [3]

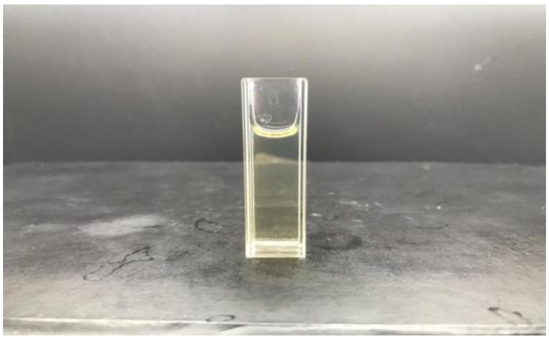

Fig.7. Ag doped CD under daylight

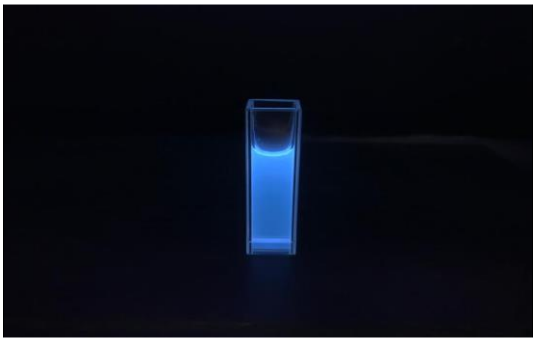

Fig.8. Ag doped CD under UV

IV. The synthesis of silver nanocomposite can be obtained through the following ways: -

I. Hydro-thermal treatment with the L-Cysteine at 200°C

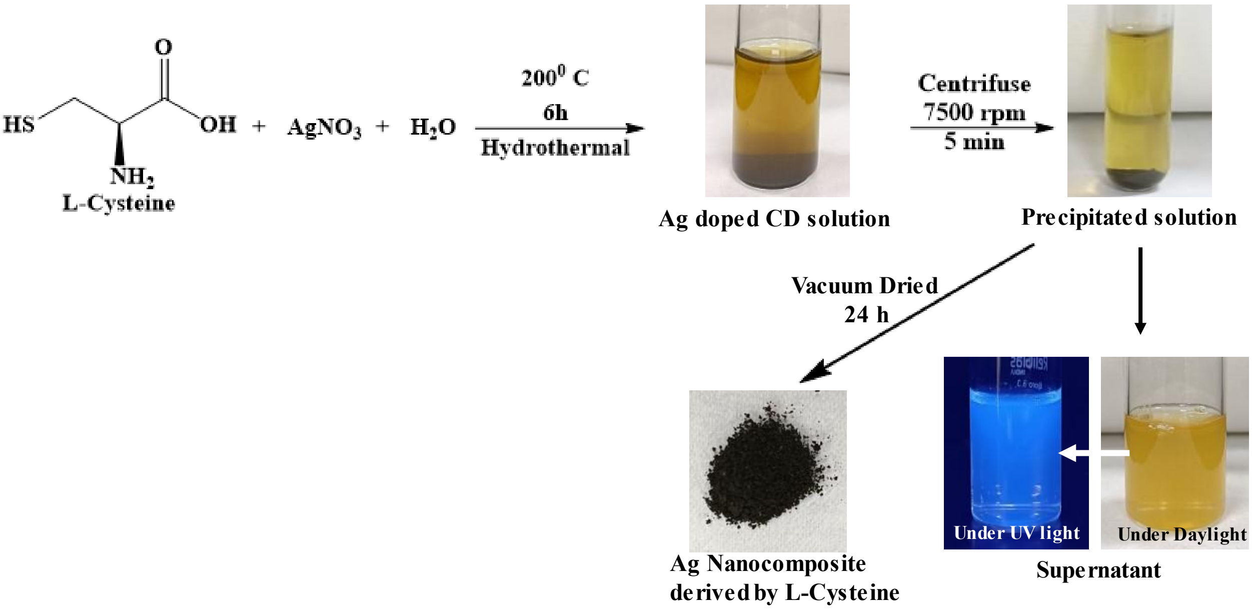

Fig.9. Synthetic scheme of Ag Nanocomposite derived by L-Cysteine

200 mg of L-Cysteine and 100 mg of $AgNO_3$ is added to 12.5 ml of water and the solution was sonicated for five minutes at room temperature. The solution was then transferred to a stainless steel autoclave with a Teflon lining, which was subsequently baked for six hours at 200°C. This resulted in a yellow-coloured solution which was further centrifuged to obtain the precipitate. Then the supernatant was segregated from the precipitate and the resultant supernatant was found to be a Carbon dot showing a blue fluorescent. Moreover, the precipitate was washed and dried to obtain a solid powder. A similar observation was found by following the standard parameters of the reaction as earlier reactions with only a variation in pH level (pH = 7.4).

II. Hydro-thermal treatment with the mixture of L-Cysteine and Citric acid at 200°C

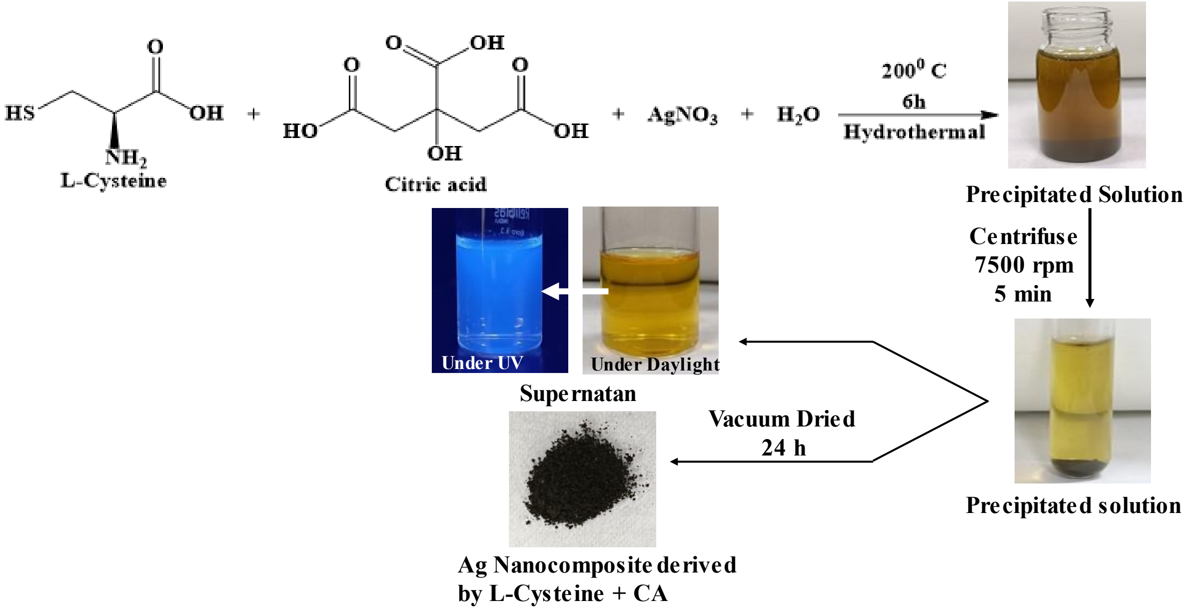

Fig.10. Synthetic scheme of Ag Nanocomposite derived by L-Cysteine + CA

75 mg L-Cysteine and 100 mg $AgNO_3$ were dissolved in 2.5 mL DI water and agitated for 1 hour at room temperature. To make the solution 12.5 mL, 125 mg citric acid was added to the aforesaid solution, along with DI water. The solution was then transferred to a stainless steel autoclave with a Teflon lining, which was subsequently baked for six hours at 200°C. This resulted in a yellow-coloured solution which was further centrifuged to obtain the precipitate. Then the supernatant was segregated from the precipitate and the resultant supernatant was found to be a Carbon dot showing a blue fluorescent. Moreover, the precipitate was washed and dried to obtain a solid powder. A similar observation was found by following the standard parameters of the reaction as earlier reactions with only a variation in pH level (pH =7.4) and the reaction time (shifted to 20 hours).

III. Thermal treatment with the L-Cysteine + Citric acid carbon dot at 100°C

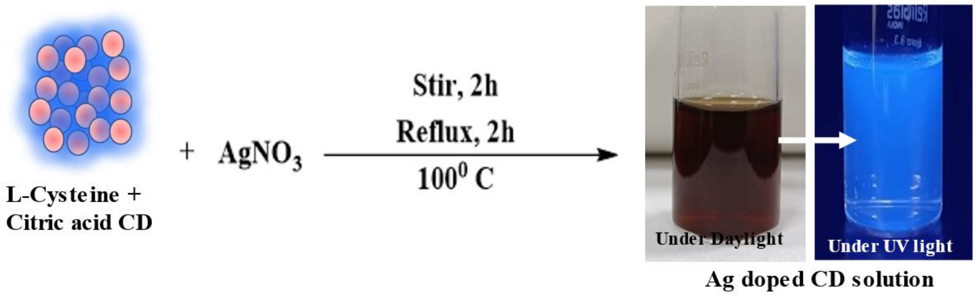

Fig.11. Synthetic scheme of Ag doped CD

Firstly, the synthesis of L-Cysteine + Citric acid carbon dot was obtained. Then 10 ml of Carbon dot is taken in a round bottom flask and 16.7 mg of AgNO3 is added to it and the solution was stirred for 2 hours at room temperature. The resultant solution was subsequently refluxed at 100°C for two hours. The solution of CD was Dark yellow in daylight, and exhibited blue fluorescence under UV light. In this reaction no precipitate was formed which shows that the silver sulphide nanoparticles is not formed but the silver doped carbon dot is formed.

IV. Thermal treatment with the L-Cysteine carbon dot at 100°C

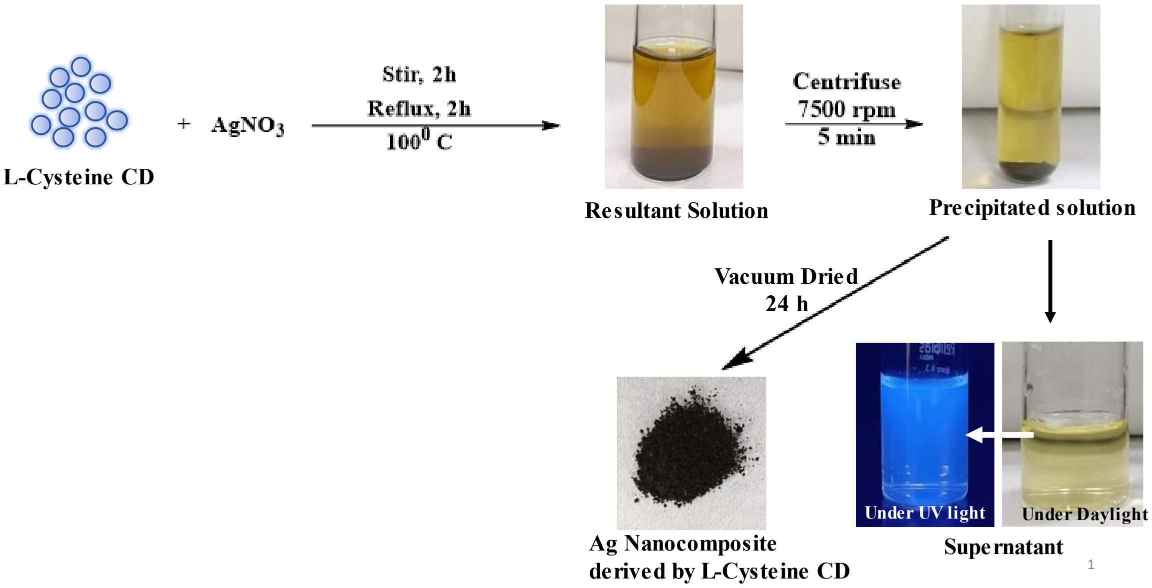

Fig.12. Synthetic scheme of Ag Nanocomposite derived by L-Cysteine CD

Firstly, the synthesis of L-Cysteine carbon dot was obtained. Then 10 ml of Carbon dot is taken in a round bottom flask and 16.7 mg of $AgNO_3$ is added to it and the solution was stirred for 2 hours at room temperature. The resultant solution was subsequently refluxed at 100°C for two hours. This resulted in a yellow-coloured solution which was further centrifuged to obtain the precipitate. Then the supernatant was segregated from the precipitate and the resultant supernatant was found to be a Carbon dot showing a blue fluorescent. Moreover, the precipitate was washed and dried to obtain a solid powder.

C. CHARACTERIZATION

1. OPTICAL PROPERTIES

a. Sodium citrate capped silver nanoparticles

Figure 13 shows the UV–vis spectrum of freshly produced citrate capped silver nanoparticles. At 400 nm, the characteristic surface plasmon absorption peak can be seen. The Ag NPs produce comparable spectrum after two months, indicating that they are stable over time. The data was well matched with the literature.[8]

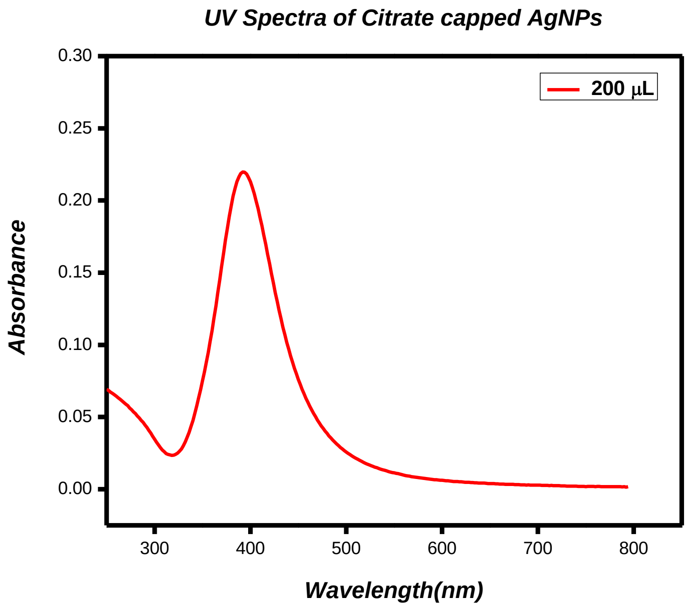

Fig.13. UV spectrum of citrate capped Ag NPs

b. Polyvinyl Pyrrolidone (PVP) capped silver nanoparticles

Figure 14 shows the UV–vis spectrum of freshly manufactured PVP capped silver nanoparticles. At 400 nm, the characteristic surface plasmon absorption peak can be seen. Our generated silver nanoparticle is proven to be stable after several weeks. The data was well matched with the literature.[8]

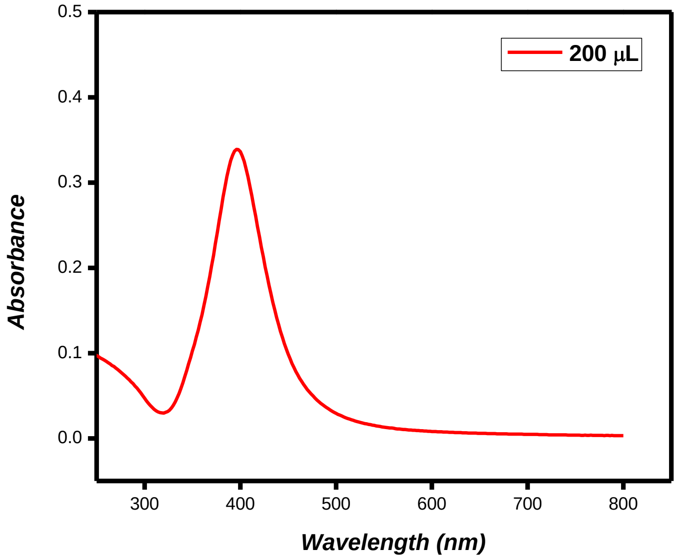

Fig.14. UV spectrum of PVP capped AgNPs

c. Silver doped carbon dot

UV–Vis absorption spectroscopy and fluorescence spectroscopy were used to investigate the optical characteristics of CD, as shown in figs. 15 and 16. The CD solution was pale yellow in the daylight. Solutions fluoresced blue when exposed to UV light (365 nm). CD exhibits one noticeable absorption peak at 362 nm, which was linked to the n-π* transition in the UV–Vis spectrum. CD emission wavelengths were not dependent on excitation wavelengths, with optical excitation wavelengths of 360 nm and emission wavelengths of 452 nm, respectively. The data was well matched with the literature. [3]

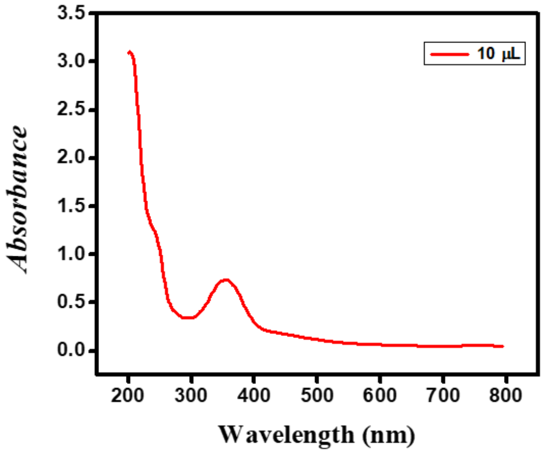

Fig.15. UV spectrum of Ag doped CDs

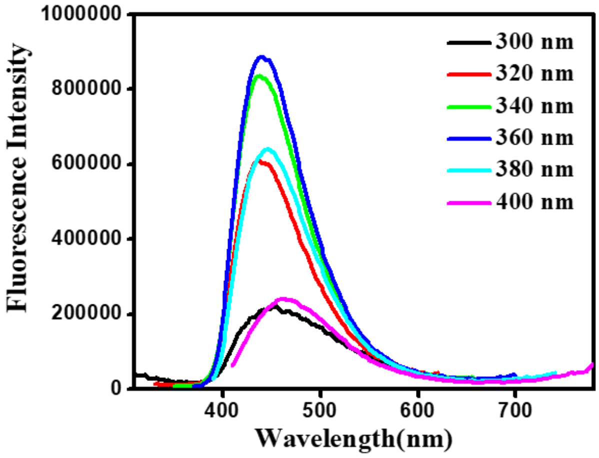

Fig.16. Fluorescence emission spectrum of Ag doped CDs

d. UV spectrum of Ag nanocomposite under following conditions

I. L-Cysteine with $AgNO_3$ at 200°C

Firstly, characterization of Ag nanocomposite was performed using UV–visible spectrophotometric analysis. Fig.17(a) shows the UV Spectrum of L-Cysteine CD showing absorption peak around 260 nm. Fig.17(b) shows the UV Spectrum of Supernatant showing similar kind of spectrum as L-Cysteine CD which reveal that our Supernatant obtained is a carbon dot and also further confirmed by the Fluorescence Spectroscopy. Fig.17(c) shows the UV Spectrum of Synthesized silver nanocomposite showing the absorption peak around 520 nm. The UV demonstrates that the synthesis of silver nanocomposite was successfully achieved through this process.

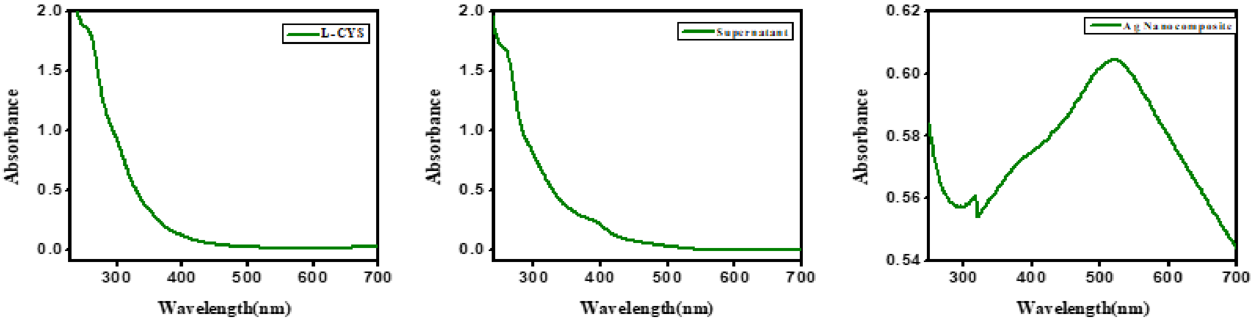

Fig.17. (a)UV spectrum of L-Cysteine CD (b)UV spectrum of supernatant formed by L-Cysteine at 200^0 C (c)UV spectrum of Ag nanocomposite derived by L-Cysteine at 200^0 C

II. L-Cysteine + Citric acid with $AgNO_3$ at 200°C

Firstly, characterization of Ag nanocomposite was performed using UV–visible spectrophotometric analysis. Fig.18(a) shows the UV Spectrum of L-Cysteine + Citric acid CD showing absorption peak around 354 nm. Fig.18(b) shows the UV Spectrum of Supernatant showing similar kind of spectrum as L-Cysteine + Citric acid CD which reveal that our Supernatant obtained is a carbon dot and also further confirmed by the Fluorescence Spectrum. Fig.18(c) shows the UV Spectrum of Synthesized silver nanocomposite showing the absorption peak around 520 nm. The UV demonstrates that the synthesis of silver nanocomposite was successfully achieved through this process.

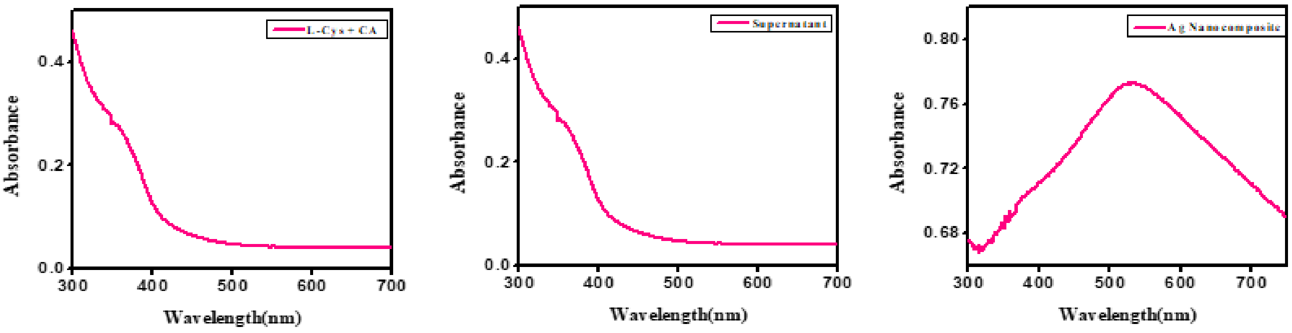

Fig.18. (a)UV spectrum of L-Cysteine + CA CD (b)UV spectrum of supernatant formed by L-Cysteine + CA at 200^0 C (c)UV spectrum of Ag nanocomposite derived by L-Cysteine + CA at 200^0 C

III. L-Cysteine CD with $AgNO_3$ at 100°C

Firstly, characterization of Ag nanocomposite was performed using UV–visible spectrophotometric analysis. Fig.19(a) shows the UV Spectrum of L-Cysteine CD showing absorption peak around 260 nm. Fig.19(b) shows the UV Spectrum of Supernatant showing similar kind of spectrum as L-Cysteine CD which reveal that our Supernatant obtained is a carbon dot and also further confirmed by the Fluorescence Spectrum. Fig.19(c) shows the UV Spectrum of Synthesized silver nanocomposite showing the absorption peak around 520 nm. The UV demonstrates that the synthesis of silver nanocomposite was successfully achieved through this process.

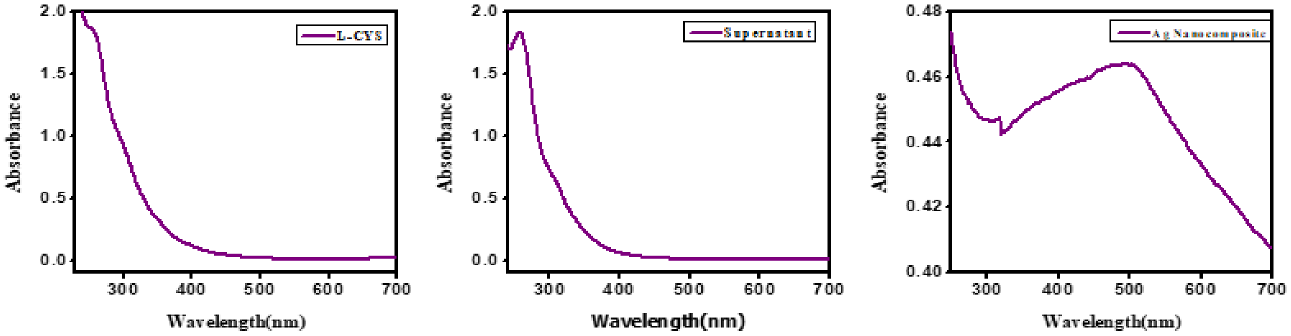

Fig.19. (a)UV spectrum of L-Cysteine CD (b)UV spectrum of supernatant formed by L-Cysteine CD at 100^0 C (c)UV spectrum of Ag nanocomposite derived by L-Cysteine CD at 100^0 C

IV. L-Cysteine + Citric acid CD with $AgNO_3$ at 100°C

Firstly, characterization of Ag nanocomposite was performed using UV–visible spectrophotometric analysis. Fig.20(a) shows the UV Spectrum of L-Cysteine + Citric acid CD showing absorption peak around 354 nm. Fig.20(b) shows the UV Spectrum of Silver doped carbon dot showing similar kind of spectrum as L-Cysteine + Citric acid CD which reveal that our Solution obtained is a silver doped carbon dot and also further confirmed by the Fluorescence Spectrum.

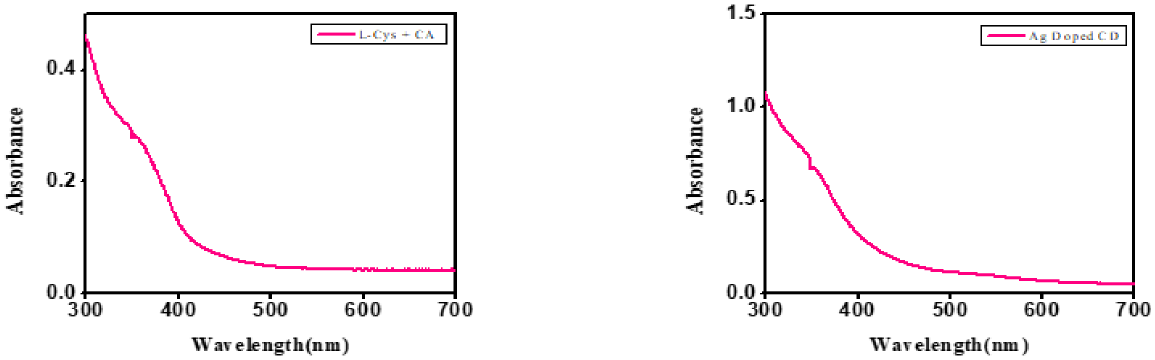

Fig.20. (a)UV spectrum of L-Cysteine + CA CD (b)UV spectrum of supernatant formed by L-Cysteine CD at 100^0 C

V. L-Cysteine with $AgNO_3$ at 200°C (Adjusting pH to 7.4)

Firstly, characterization of Ag nanocomposite was performed using UV–visible spectrophotometric analysis. Even with a variation in pH scale, similar kind of reaction is observed. Fig.21(a) shows the UV Spectrum of L-Cysteine CD showing absorption peak around 260 nm. Fig.21(b) shows the UV Spectrum of Supernatant showing similar kind of spectrum as L-Cysteine CD which reveal that our Supernatant obtained is a carbon dot and also further confirmed by the Fluorescence Spectrum.

Fig.21(c) shows the UV Spectrum of Synthesized silver nanocomposite showing the absorption peak at 520 nm. The UV demonstrates that the synthesis of silver nanocomposite was successfully achieved through this process.

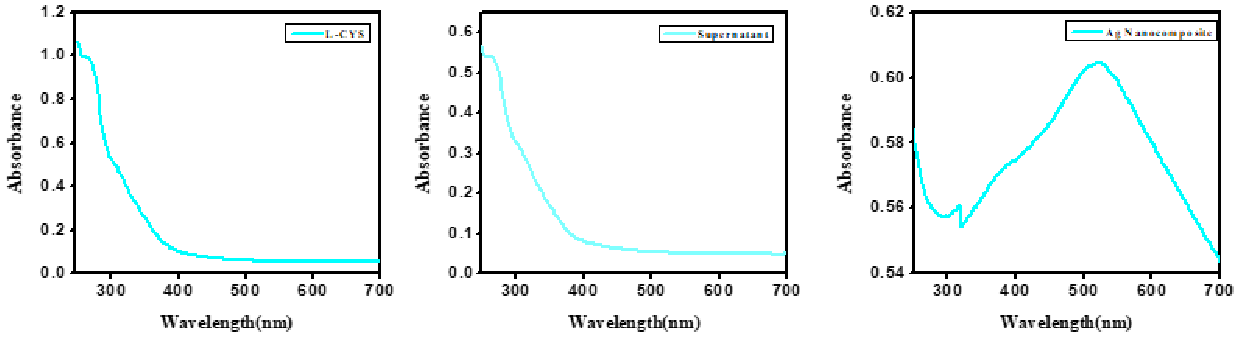

Fig.21. (a)UV spectrum of L-Cysteine CD at pH 7.4 (b)UV spectrum of supernatant formed by L-Cysteine at pH 7.4 (c)UV spectrum of Ag nanocomposite derived by L-Cysteine at pH 7.4

VI. L-Cysteine + Citric acid with AgNO$_3$ at 200°C (Adjusting pH to 7.4)

Firstly, characterization of Ag nanocomposite was performed using UV–visible spectrophotometric analysis. with a variation in pH scale, similar kind of reaction is observed. Fig.22(a) shows the UV Spectrum of L-Cysteine + Citric acid CD showing absorption peak around 334 nm. Fig.22(b) shows the UV Spectrum of Supernatant showing similar kind of spectrum as L-Cysteine + Citric acid CD which reveal that our Supernatant obtained is a carbon dot and also further confirmed by the Fluorescence Spectrum. Fig.22(c) shows the UV Spectrum of Synthesized silver nanocomposite showing the absorption peak at 520 nm. The UV demonstrates that the synthesis of silver nanocomposite was successfully achieved through this process.

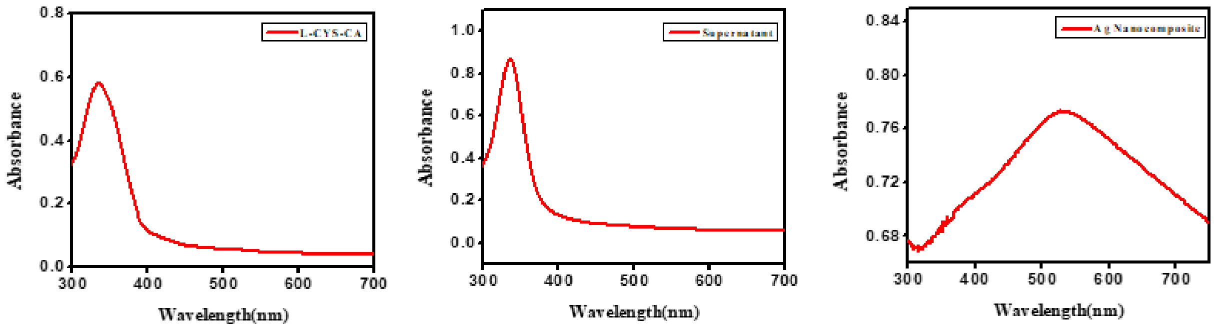

Fig.22. (a)UV spectrum of L-Cysteine + CA CD at pH 7.4 (b)UV spectrum of supernatant formed by L-Cysteine + CA at pH 7.4 (c)UV spectrum of Ag nanocomposite derived by L-Cysteine + CA at pH 7.4

VII. L-Cysteine + Citric acid with $AgNO_3$ at 200°C (Adjusting reaction time for 20 hours)

Firstly, characterization of Ag nanocomposite was performed using UV–visible spectrophotometric analysis. Even with a variation in time, similar kind of reaction is observed. Fig.23(a) shows the UV Spectrum of L-Cysteine + Citric acid CD showing absorption peak around 354 nm. Fig.23(b) shows the UV Spectrum of Supernatant showing similar kind of spectrum as L-Cysteine + Citric acid CD which reveal that our Supernatant obtained is a carbon dot and also further confirmed by the Fluorescence Spectrum. Fig.23(c) shows the UV Spectrum of Synthesized silver nanocomposite showing the absorption peak at 520 nm. The UV demonstrates that the synthesis of silver nanocomposite was successfully achieved through this process.

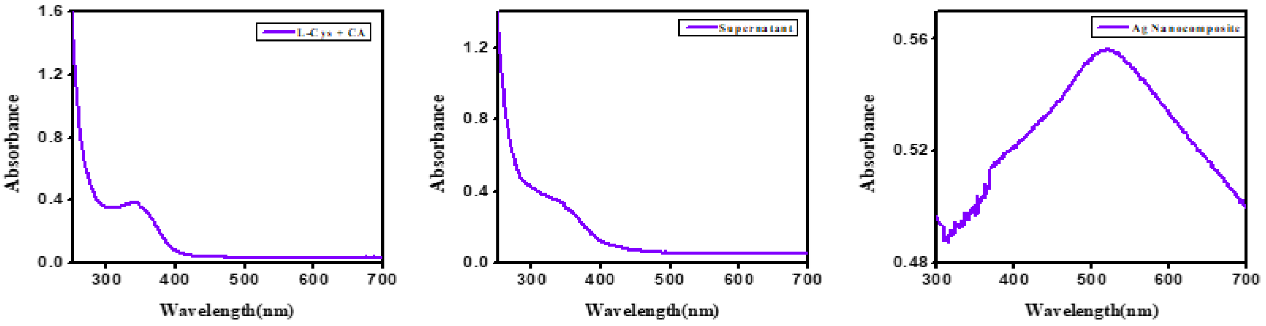

Fig.23. (a)UV spectrum of L-Cysteine + CA CD at 20 hours (b)UV spectrum of supernatant formed by L-Cysteine + CA at 20 hours (c)UV spectrum of Ag nanocomposite derived by L-Cysteine + CA at 20 hours

e. Fluorescence spectrum of carbon dot under following conditions

I. L-Cysteine carbon dot

Post the successful characterisation of the UV spectrum, we further studied it under fluorescence spectrum. Firstly, the excitation of Carbon dot was done at 320 nm and the emission wavelength was received at 398 nm. Then, the excitation wavelength was gradually increased and a red shift in the spectrum was observed. This demonstrates that Carbon dot shows excitation dependent emission which further reveals that Carbon dot are non-uniform in size. The highest emission peak was observed at 412 nm while the excitation wavelength was at 340 nm.

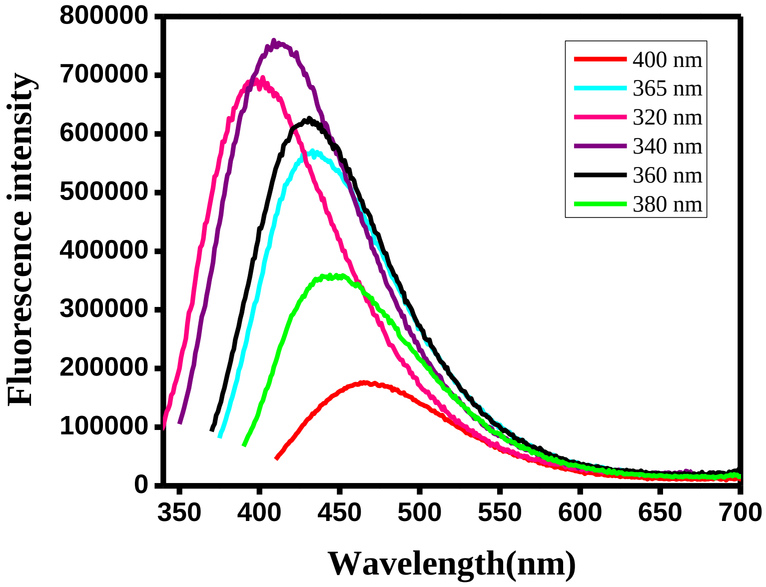

Fig.24. Fluorescence spectrum of L-Cysteine carbon dot.

II. L-Cysteine + Citric acid carbon dot

Post the successful characterisation of the UV spectrum, we further studied it under fluorescence spectrum. Firstly, the excitation of Carbon dot was done at 300 nm and the emission wavelength was received at 420 nm. Then, the excitation wavelength was gradually increased and a red shift in the spectrum was not observed. This demonstrates that Carbon dot do not show excitation dependent emission which further reveals that Carbon dot are uniform in size.

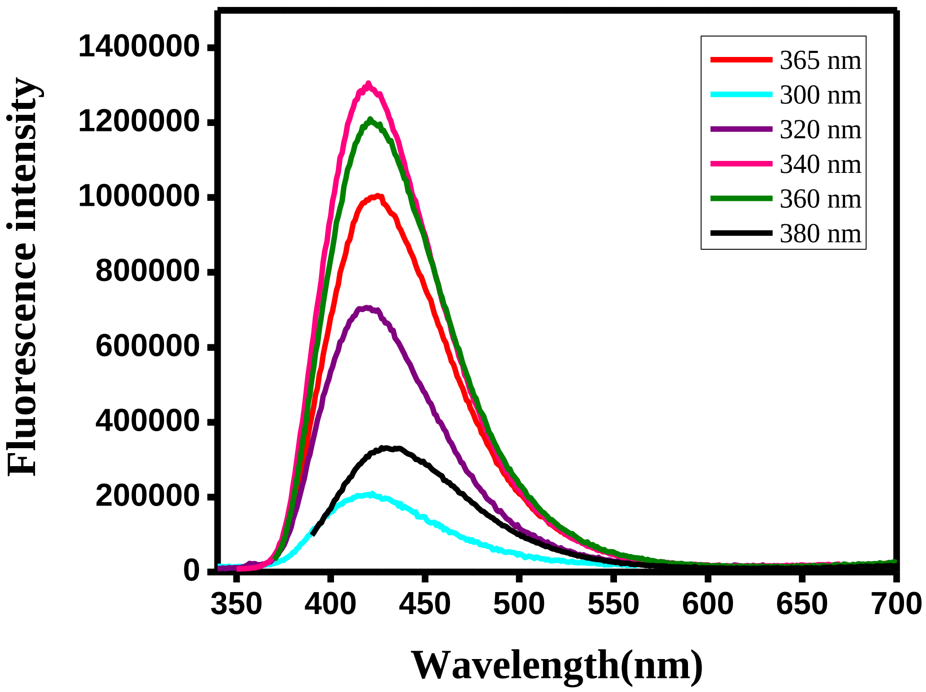

Fig.25. Fluorescence spectrum of L-Cysteine + Citric acid carbon dot.

III. L-Cysteine with $AgNO_3$ at 200°C (supernatant)

Post the successful characterisation of the UV spectrum, we further studied it under fluorescence spectrum. Firstly, the excitation of Carbon dot was done at 320 nm and the emission wavelength was received at 400 nm. Then, the excitation wavelength was gradually increased and a red shift in the spectrum was observed. This demonstrates that Carbon dot shows excitation dependent emission which further reveals that Carbon dot are non-uniform in size. The highest emission peak was observed at 412 nm while the excitation wavelength was at 340 nm. The only distinction between L-Cysteine Carbon dot and supernatant was found to be in its fluorescence intensity level where the supernatant shows remarkably low intensity as compared to the Carbon dot.

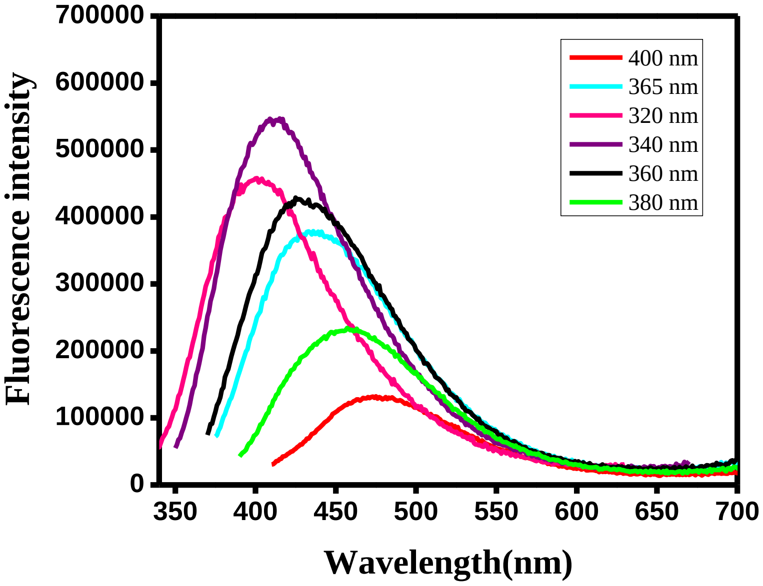

Fig.26. Fluorescence spectrum of Supernatant

IV. L-Cysteine CD with $AgNO_3$ at 100°C (supernatant)

Post the successful characterisation of the UV spectrum, we further studied it under fluorescence spectrum. Firstly, the excitation of Carbon dot was done at 320 nm and the emission wavelength was received at 398 nm. Then, the excitation wavelength was gradually increased and a red shift in the spectrum was observed. This demonstrates that Carbon dot shows excitation dependent emission which further reveals that Carbon dot are non-uniform in size.

The highest emission peak was observed at 412 nm while the excitation wavelength was at 340 nm. The only distinction between L-Cysteine Carbon dot and supernatant was found to be in its fluorescence intensity level where the supernatant shows remarkably low intensity as compared to the Carbon dot.

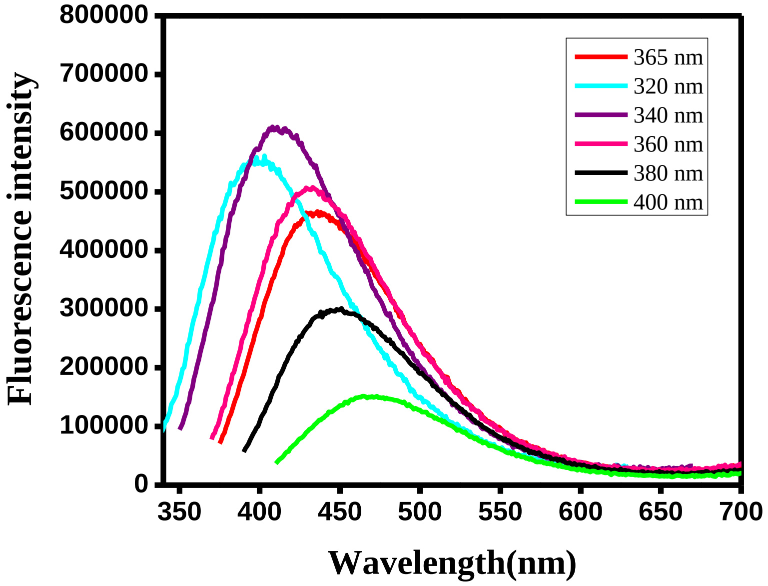

Fig.27. Fluorescence spectrum of Supernatant.

V. L-Cysteine + Citric acid with $AgNO_3$ at 200°C (supernatant)

Post the successful characterisation of the UV spectrum, we further studied it under fluorescence spectrum. Firstly, the excitation of Carbon dot was done at 300 nm and the emission wavelength was received at 427 nm. Then, the excitation wavelength was gradually increased and a red shift in the spectrum was observed. This demonstrates that Carbon dot show excitation dependent emission which further reveals that Carbon dot are non-uniform in size. Besides a remarkable difference observed in the intensity level of fluorescence, it was also observed that the size of Carbon dot was non-uniform as compared to the uniform size observed in L-Cysteine + Citric Acid Carbon dot. This difference in size occurs due to the interaction of Ag^+ ions.

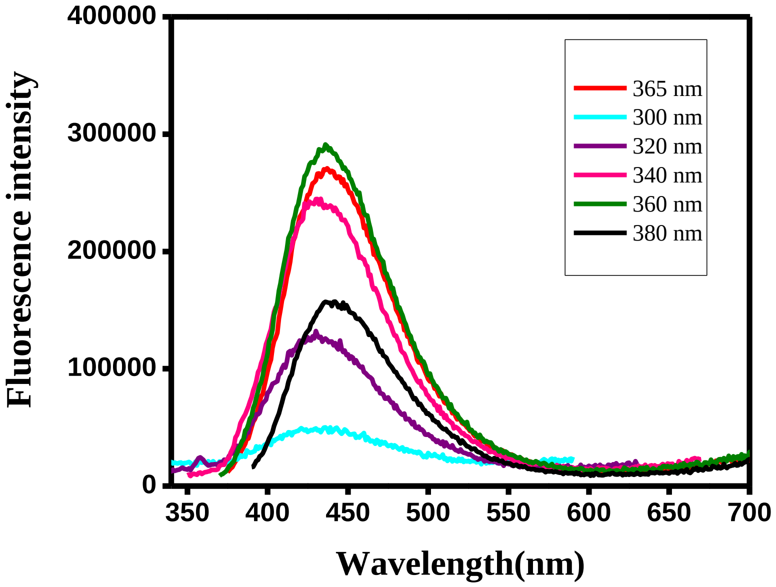

Fig.28. Fluorescence spectrum of Supernatant

VI. L-Cysteine + Citric acid CD with $AgNO_3$ at 100°C

Post the successful characterisation of the UV spectrum, we further studied it under fluorescence spectrum. Firstly, the excitation of Carbon dot was done at 300 nm and the emission wavelength was received at 418 nm. Then, the excitation wavelength was gradually increased and a red shift in the spectrum was observed. This demonstrates that Carbon dot do not show excitation dependent emission which further reveals that Carbon dot are uniform in size.

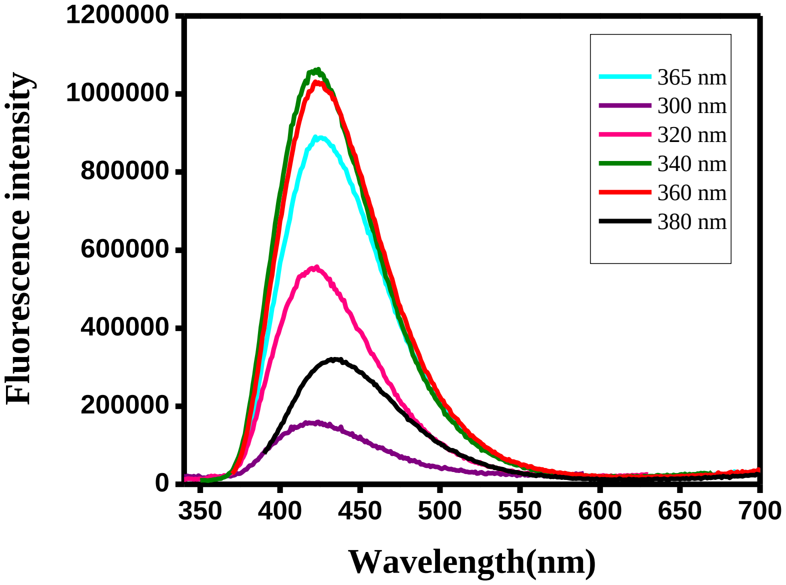

Fig.29. Fluorescence spectrum of Supernatant

VII. L-Cysteine CD at pH=7.4 (supernatant)

Post the successful characterisation of the UV spectrum, we further studied it under fluorescence spectrum. Firstly, the excitation of Carbon dot was done at 300 nm and the emission wavelength was received at 400 nm. Then, the excitation wavelength was gradually increased and a red shift in the spectrum was observed. This demonstrates that Carbon dot shows excitation dependent emission which further reveals that Carbon dot are non-uniform in size. The highest emission peak was observed at 418 nm while the excitation wavelength was at 340 nm.

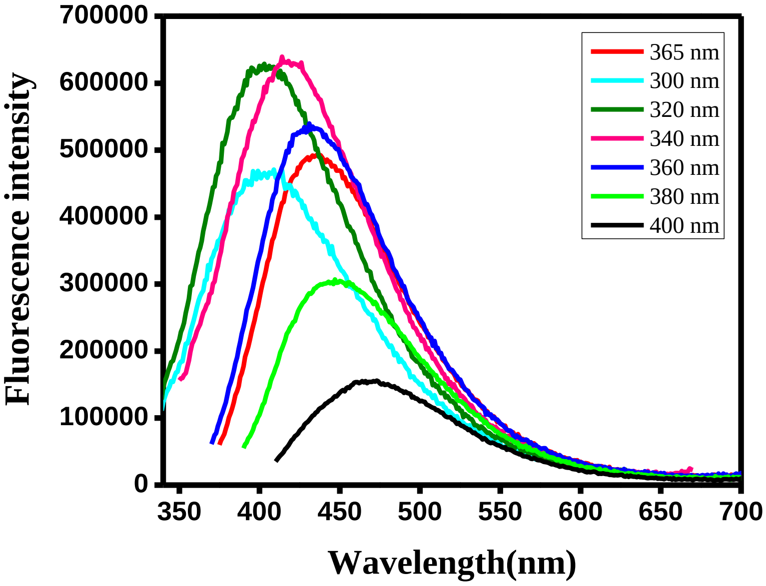

Fig.30. Fluorescence spectrum of L-Cysteine CD at pH 7.4

VIII. L-Cysteine + Citric acid CD at pH=7.4 (supernatant)

Post the successful characterisation of the UV spectrum, we further studied it under fluorescence spectrum. Firstly, the excitation of Carbon dot was done at 300 nm and the emission wavelength was received at 438 nm. Then, the excitation wavelength was gradually increased and a red shift in the spectrum was not observed. This demonstrates that Carbon dot do not show excitation dependent emission which further reveals that Carbon dot are uniform in size.

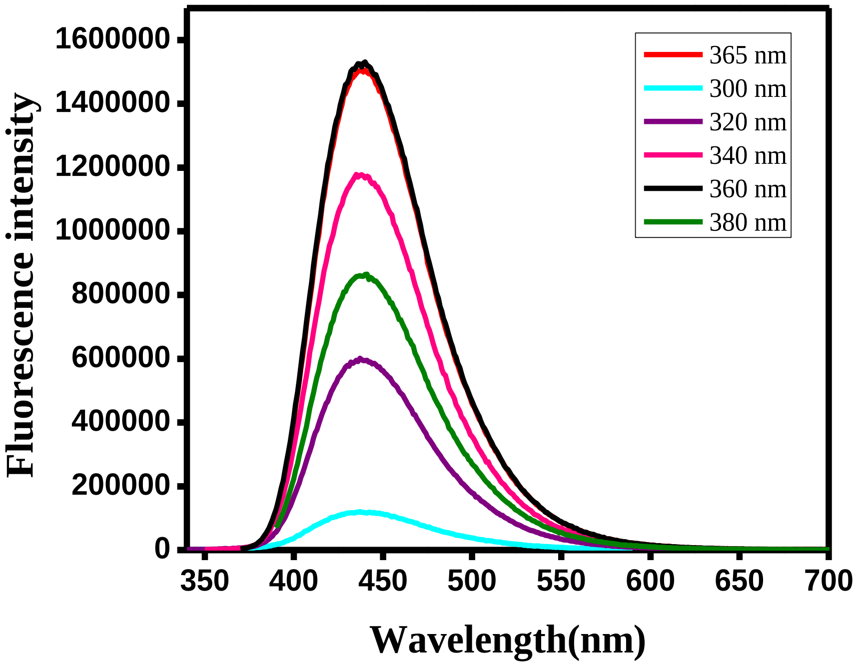

Fig.31. Fluorescence spectrum of L-Cysteine + CA at pH 7.4

IX. L-Cysteine with $AgNO_3$ at 200°C at pH=7.4 (supernatant)

Post the successful characterisation of the UV spectrum, we further studied it under fluorescence spectrum. Firstly, the excitation of Carbon dot was done at 300 nm and the emission wavelength was received at 417 nm. Then, the excitation wavelength was gradually increased and a red shift in the spectrum was observed. This demonstrates that Carbon dot shows excitation dependent emission which further reveals that Carbon dot are non-uniform in size. The highest emission peak was observed at 424 nm while the excitation wavelength was at 340 nm. The only distinction between L-Cysteine Carbon dot and supernatant was found to be in its fluorescence intensity level where the supernatant shows remarkably low intensity as compared to the Carbon dot.

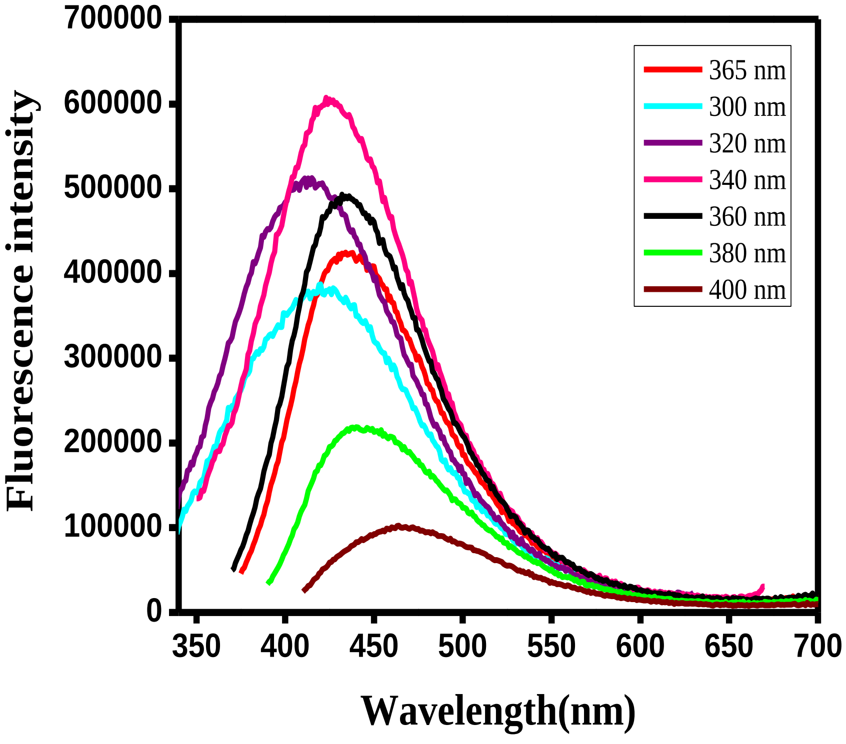

Fig.32. Fluorescence spectrum of Supernatant

X. L-Cysteine + Citric acid with $AgNO_3$ at 200°C at pH=7.4 (supernatant)

Post the successful characterisation of the UV spectrum, we further studied it under fluorescence spectrum. Firstly, the excitation of Carbon dot was done at 300 nm and the emission wavelength was received at 411 nm. Then, the excitation wavelength was gradually increased and a red shift in the spectrum was observed. This demonstrates that Carbon dot show excitation dependent emission which further reveals that Carbon dot are non-uniform in size. Besides a remarkable difference observed in the intensity level of fluorescence, it was also observed that the size of Carbon dot was non-uniform as compared to the uniform size observed in L-Cysteine + Citric Acid Carbon Dot. This difference in size occurs due to the interaction of Ag^+ ions.

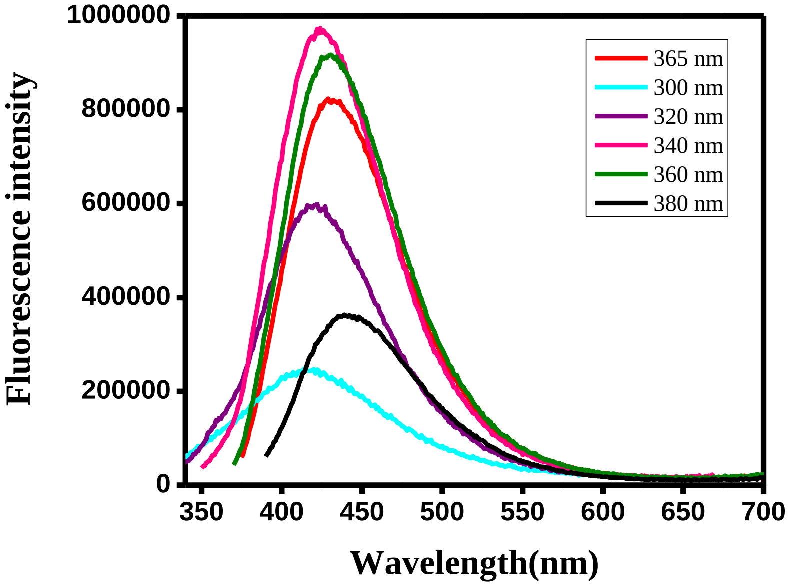

Fig.33. Fluorescence spectrum of Supernatant

2. FE-SEM

a. Sodium citrate capped Silver Nanoparticles

The particle size dispersal and shape of the as-synthesised Ag NPs were measured using a FE-SEM, as shown in fig.34. The development of spherical Ag NPs produced with citrate capping agent was clearly seen in the FE-SEM pictures. Citrate-capped Ag NPs were found to agglomerate into bigger particles to a small amount. Studies of synthesised Ag NPs using a transmission electron microscope (TEM) have yet to be completed.

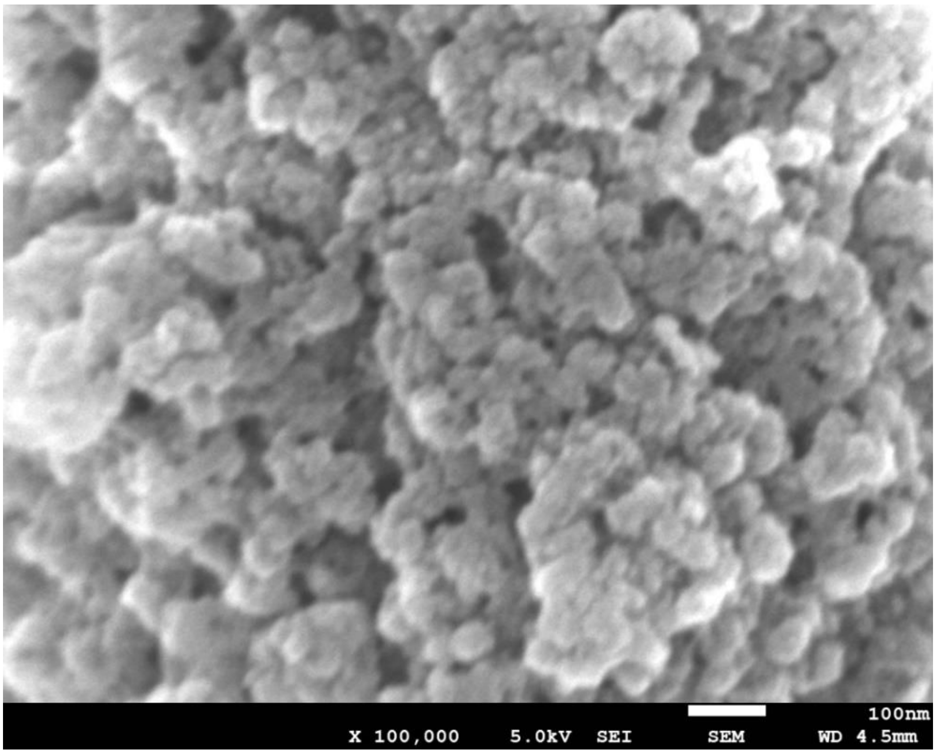

Fig.34. SEM image of citrate capped AgNPs

b. Polyvinyl pyrrolidone (PVP) capped Silver Nanoparticles

The particle size distribution and shape of the as-synthesised Ag NPs were measured using a field emission scanning electron microscope (FE-SEM), as shown in fig.35. The development of spherical Ag NPs synthesised with PVP capping agent was clearly visible in FESEM pictures.

Studies of synthesised Ag NPs using a transmission electron microscope (TEM) have yet to be completed.

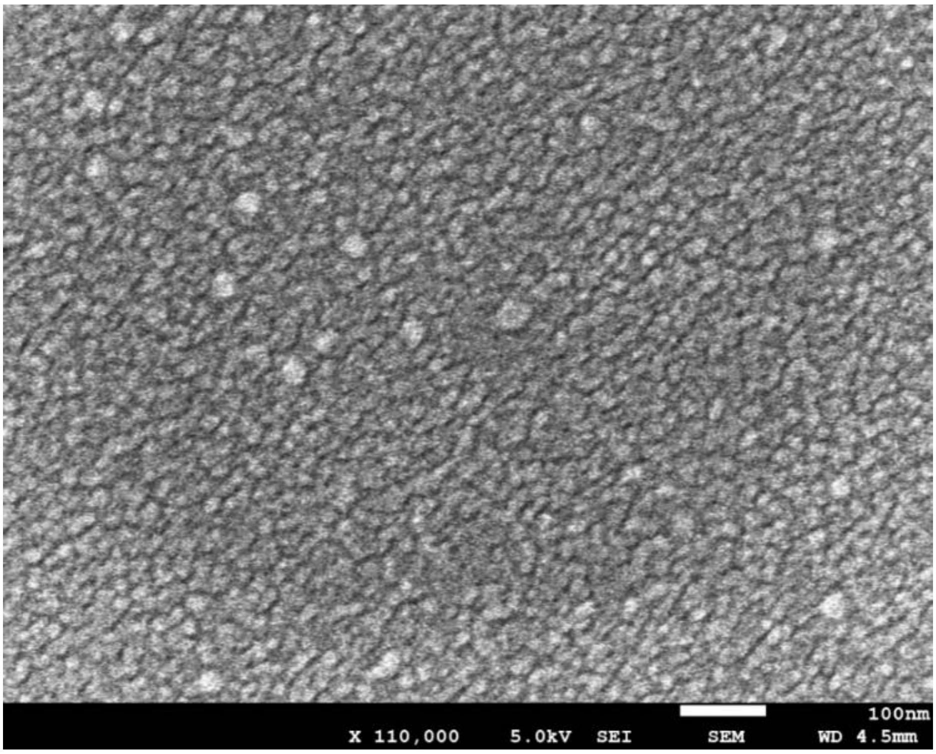

Fig.35. SEM image of PVP capped AgNPs

c. Silver doped Carbon dot

The particle size distribution and shape of the as-synthesized Ag doped CD were measured using a FE-SEM, as shown in fig.36. Studies of synthesised Ag doped CD using a transmission electron microscope (TEM) have yet to be completed.

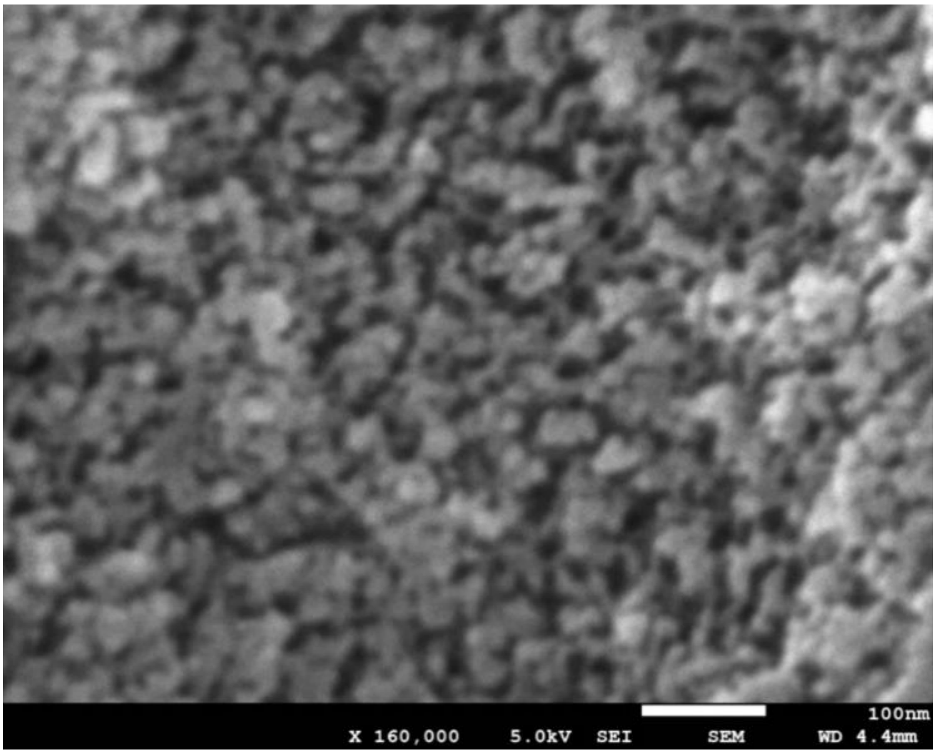

Fig.36. SEM image of Ag doped CDs

d. SEM images of silver nanocomposite under following conditions

I. L-Cysteine with $AgNO_3$ at 200°C (Ag Nanocomposite)

The particle size distribution and shape of the as-synthesised Ag nanocomposite were measured using a field emission scanning electron microscope (FE-SEM), as shown in fig.37. The development of spherical Ag nanocomposite synthesised was clearly visible in FE-SEM pictures. Studies of synthesised Ag nanocomposite using a transmission electron microscope (TEM) have yet to be completed.

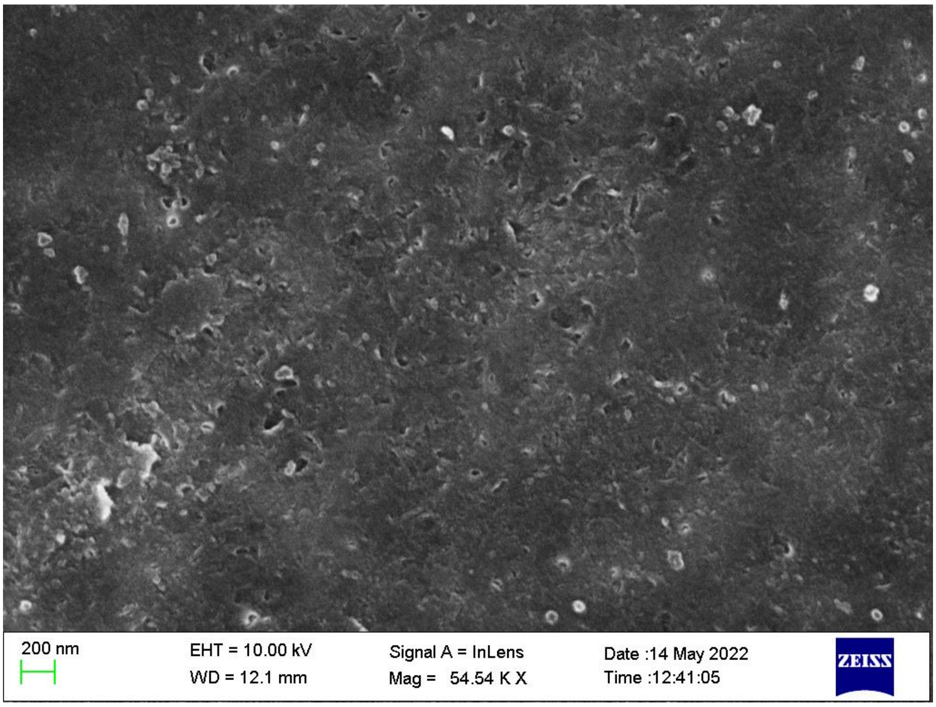

Fig.37. SEM image of Ag nanocomposite derived by L-Cysteine

3. L-Cysteine with $AgNO_3$ at 100°C (Ag nanocomposite)

The particle size distribution and shape of the as-synthesised Ag nanocomposite were measured using a field emission scanning electron microscope (FE-SEM), as shown in fig.38. The development of spherical Ag nanocomposite synthesised was clearly visible in FE-SEM pictures. Studies of synthesised Ag nanocomposite using a transmission electron microscope (TEM) have yet to be completed.

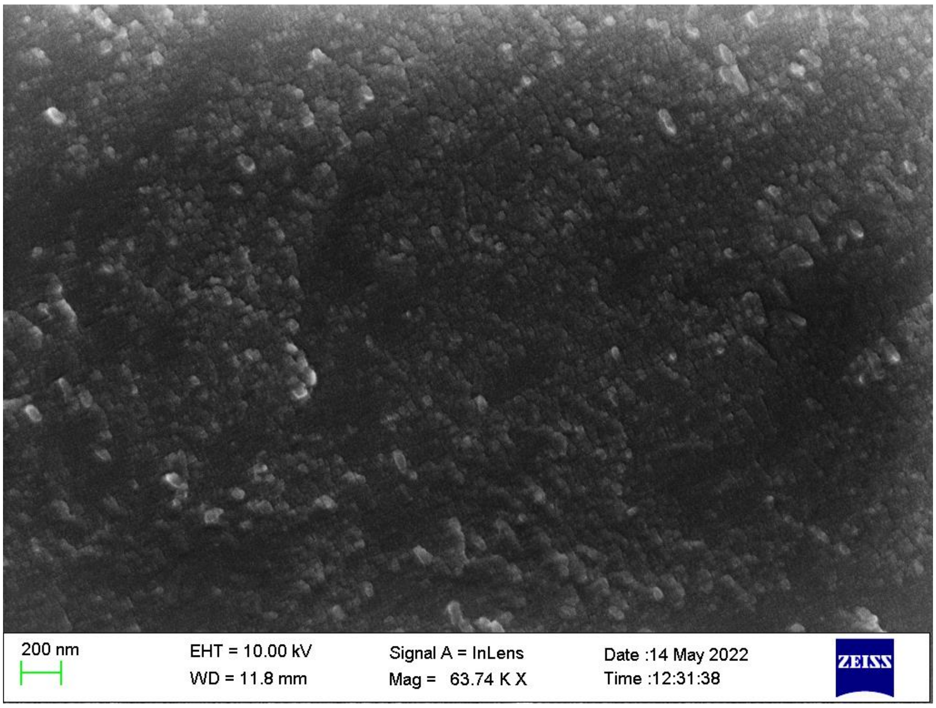

Fig.38. SEM image of Ag nanocomposite derived by L-Cysteine CD

4. L-Cysteine + Citric acid with $AgNO_3$ at 200°C (Ag nanocomposite)

The particle size distribution and shape of the as-synthesised Ag nanocomposite were measured using a field emission scanning electron microscope (FE-SEM), as shown in fig.39. Apparently, the image below suggests the aggregation of nanocomposite, however, no such observation was found in the nanocomposite formed by L-Cysteine. The Studies of synthesised Ag nanocomposite using a transmission electron microscope (TEM) have yet to be completed.

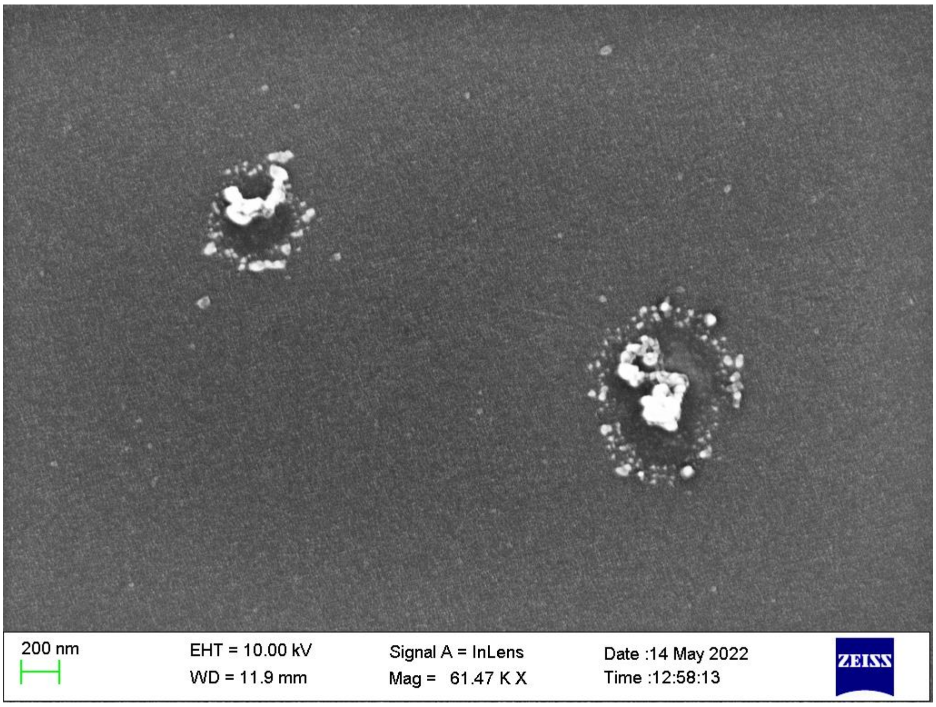

Fig.39. SEM image of Ag nanocomposite derived by L-Cysteine + CA

3. FT-IR

a. Sodium citrate capped silver nanoparticles

The presence of different functional groups in molecules are responsible for the reduction of Ag^+ and capping of silver nanoparticles was determined using FT-IR analysis. The FT-IR spectrum of citrate-capped Ag NPs in the frequency range of 4000–500 cm^{-1} are shown in Fig.16. It shows the FT-IR spectrum of free sodium citrate and citrate-capped silver nanoparticles. The existence of bands at 1620 cm^{-1} and 1384 cm^{-1}, are due to the asymmetric and symmetric C=O stretches of the carboxylate ion, respectively, as well as a large band at 3490 cm^{-1}, which is due to the O-H stretch, show that tri-sodium citrate is surface capping on silver nanoparticles. C-O stretching causes the band at 1020 cm^{-1}, while C-H strains with the alkene group causes the band at 2924.8 cm^{-1}.

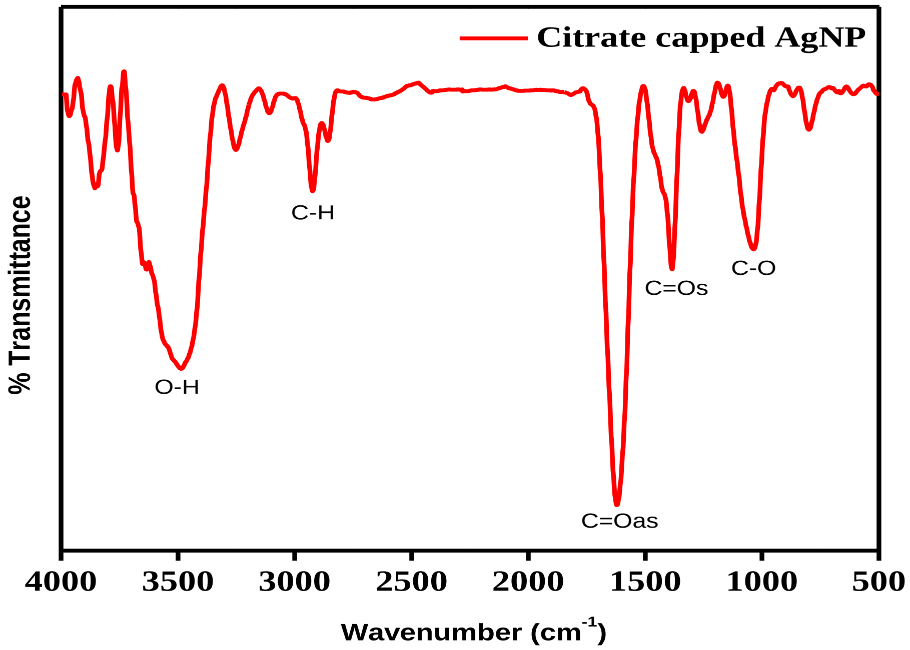

Fig.40. FT-IR spectrum of citrate capped Ag NP

b. Polyvinyl Pyrrolidone (PVP) capped silver nanoparticles

The presence of separate functional groups in molecules, responsible for Ag^+ reduction and capping of silver nanoparticles, was determined using FT-IR analysis. The FT-IR spectrum of PVP-capped Ag NPs in the frequency range of 4000–500 cm^{-1} are shown in Fig.17. Peak 3265 cm^{-1} is due to N-H stretching within amine group, while peak 2923 cm1 relates to C–H stretches with alkenes group in the FT-IR spectrum of PVP capped Ag NPs. Bond vibrations of the NO_3 group are claimed to have IR peaks at 1383 cm^{-1}. The functional unit C–N present in PVP capped Ag NPs is represented by the asymmetric and symmetric stretching vibration peak at 1020 cm^{-1}. The shifted peaks suggest that chemical absorption occurs between the N or O atoms of the PVP molecules and the surface of Ag NPs. PVP's carbonyl group stretching is indicated by a prominent absorption band at 1605 cm^{-1}, showing its presence in the sample and prevents further growth and agglomeration. The band at 800 cm^{-1} is due to >C=O stretch with strong absorption bon

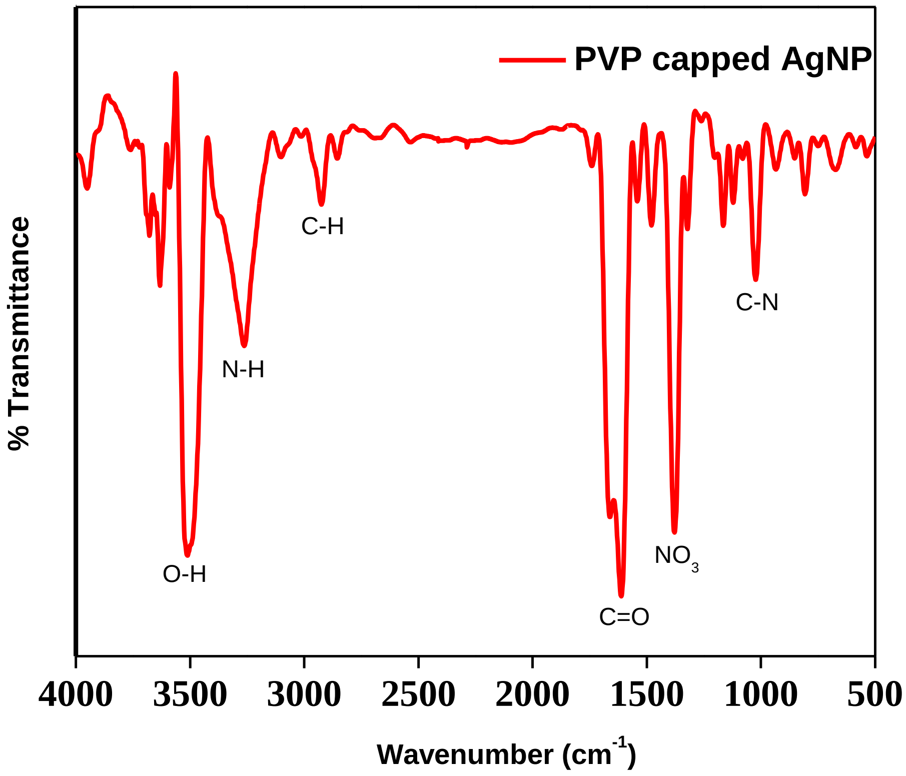

Fig.41. FT-IR spectrum of PVP capped Ag NP

c. Ag Nanocomposite

I. L-Cysteine with $AgNO_3$ at 200°C (Ag nanocomposite)

Figure 42 shows the FT-IR spectrum of Ag nanocomposite derived by L-Cysteine. The IR peak observed at 3330 cm^{-1} is due to the N-H/O-H stretching while the peak observed at 2941 cm^{-1} owes to the C-H stretching vibrations. The symmetric stretching of Carbonyl causes a sharp peak at 1641 cm^{-1} and the peak arising at 1074 cm^{-1} is caused by the asymmetric stretching of Carbonyl. The most significant peak was observed at 772 cm^{-1} which further reveals that a Silver and Sulphur bond was formed. Unlike observed in the literature where IR spectrum of L-Cysteine depicts thiol group peak around 2550 cm^{-1} which was not witnessed in the synthesis of Ag nanocomposite. This suggests that the Silver is binding with the Sulphur atom in the synthesized Ag nanocomposite.

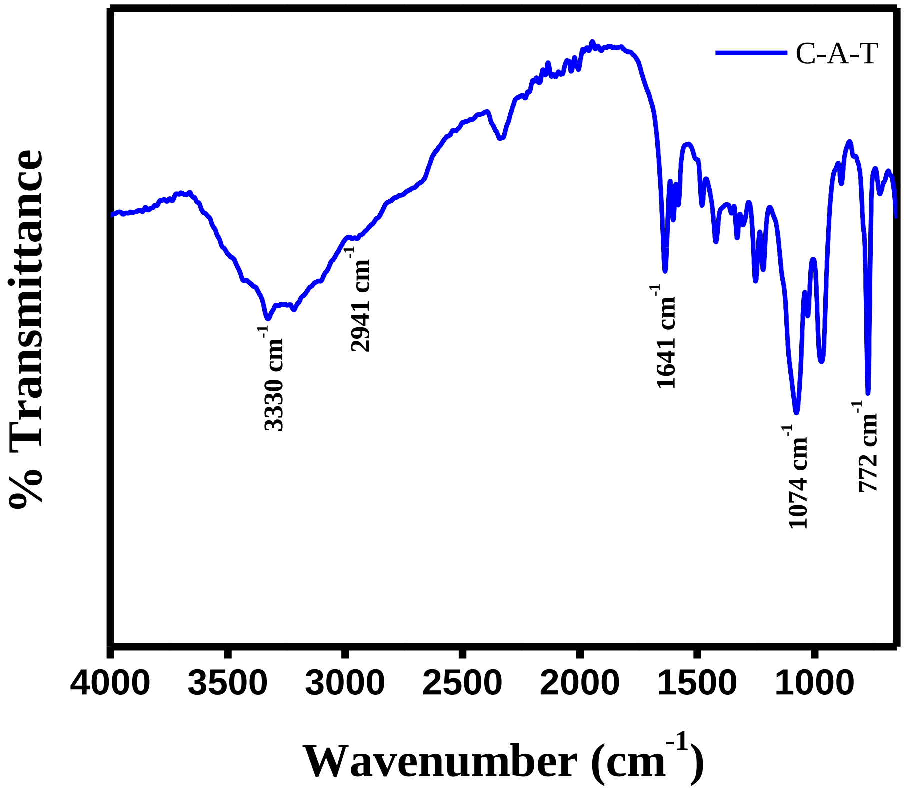

Fig.42. FT-IR spectrum of Ag nanocomposite derived by L-Cysteine

II. L-Cysteine CD with $AgNO_3$ at 100°C (Ag nanocomposite)

Figure 42 shows the FT-IR spectrum of Ag nanocomposite derived by L-Cysteine. The IR peak observed at 3326 cm^{-1} is due to the N-H/O-H stretching while the peak observed at 2926 cm^{-1} owes to the C-H stretching vibrations. The symmetric stretching of Carbonyl causes a sharp peak at 1640 cm^{-1} and the peak arising at 1076 cm^{-1} is caused by the asymmetric stretching of Carbonyl. The most significant peak was observed at 774 cm^{-1} which further reveals that a Silver and Sulphur bond was formed. Unlike observed in the literature where IR spectrum of L-Cysteine depicts thiol group peak around 2550 cm^{-1} which was not witnessed in the synthesis of Ag nanocomposite. This suggests that the Silver is binding with the Sulphur atom in the synthesized Ag nanocomposite.

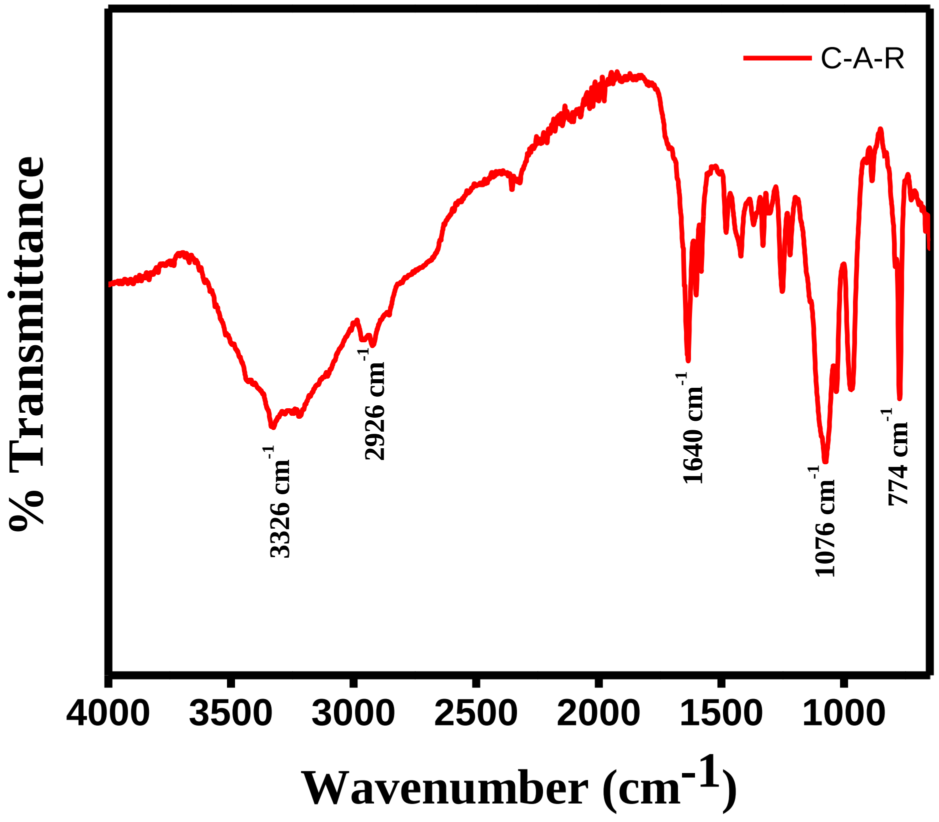

Fig.43. FT-IR spectrum of Ag nanocomposite derived by L-Cysteine CD

III. L-Cysteine + Citric acid with $AgNO_3$ at 200°C (Ag nanocomposite)

Figure 42 shows the FT-IR spectrum of Ag nanocomposite derived by L-Cysteine. The IR peak observed at 3330 cm^{-1} is due to the N-H/O-H stretching while the peak observed at 2939 cm^{-1} owes to the C-H stretching vibrations. The symmetric stretching of Carbonyl causes a sharp peak at 1641 cm^{-1} and the peak arising at 1080 cm^{-1} is caused by the asymmetric stretching of Carbonyl. The most significant peak was observed at 774 cm^{-1} which further reveals that a Silver and Sulphur bond was formed. Unlike observed in the literature where IR spectrum of L-Cysteine depicts thiol group peak around 2550 cm^{-1} which was not witnessed in the synthesis of Ag nanocomposite. This suggests that the Silver is binding with the Sulphur atom in the synthesized Ag nanocomposite.

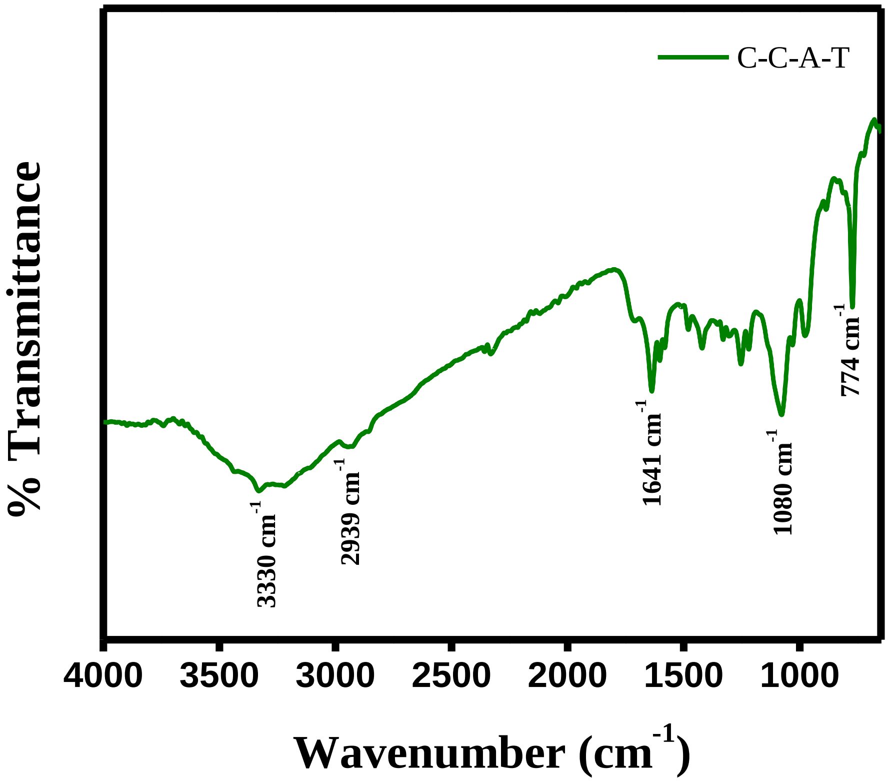

Fig.44. FT-IR spectrum of Ag nanocomposite derived by L-Cysteine + CA

4. Powder X-Ray Diffraction (PXRD)

a. Ag NPs

We made Sodium citrate capped Ag NPs, PVP capped Ag NPs, and Ag doped Carbon dot, and used PXRD to confirm their synthesis. The PXRD pattern revealed their crystalline structure, indicating that they were synthesised. In the (111), (200), (220), (311), and (222) planes, there were five well-defined typical diffraction peaks at 38.7◦, 44.3◦, 64◦, 77.4◦, and 81.8◦ conforming, respectively (Fig.45). The results demonstrate that metallic silver has a face centred cubic (fcc) crystal structure. The results of the PXRD study were very similar to what was found in the literature having (JCPDS card no. 04-0783).[8]

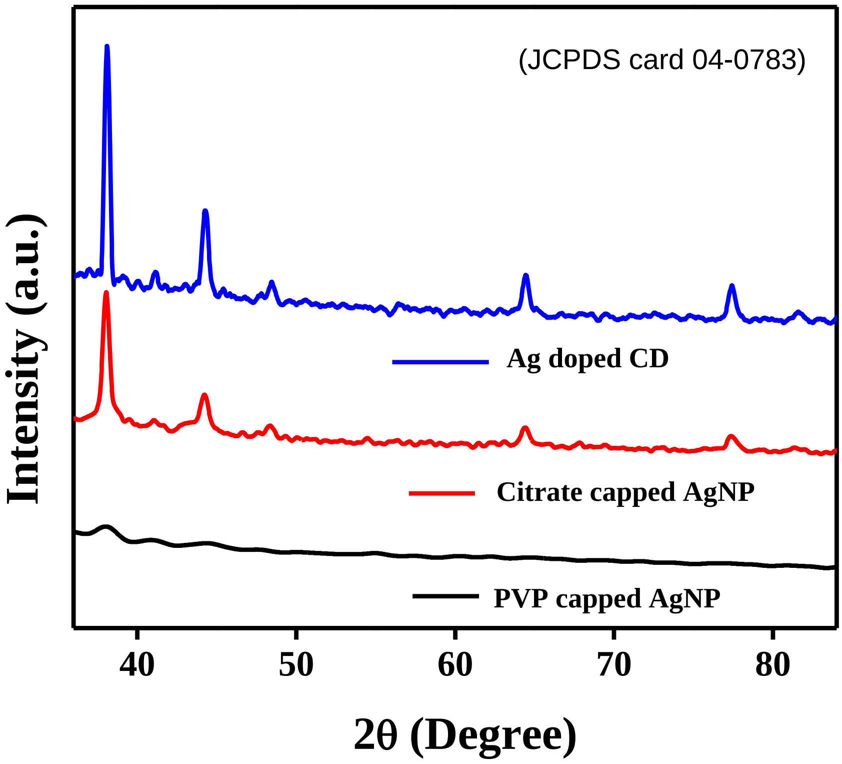

Fig.45. PXRD pattern of citrate capped Ag NPs, PVP capped Ag NPs, and Ag doped CDs

b. PXRD pattern Ag Nanocomposite under following conditions

I. L-Cysteine with $AgNO_3$ at 200°C (Ag nanocomposite)

The peaks at 22.5°, 26°, 29°, 31.7°, 34.5°, 36.9°, 40.8°, 43.5°, 45.4°, 48.6°, 53.3°, 58.3°, and 63.9° corresponding to (-101), (111), (121), (031), (200), (210), (212), (-213), (-223), and (-134) Bragg reflections, respectively, show that the silver nanocomposite formed. The silver Ag nanocomposite generated by employing L-Cysteine are crystalline in nature, according to X-ray diffraction data. The literature corroborated this information.[14]

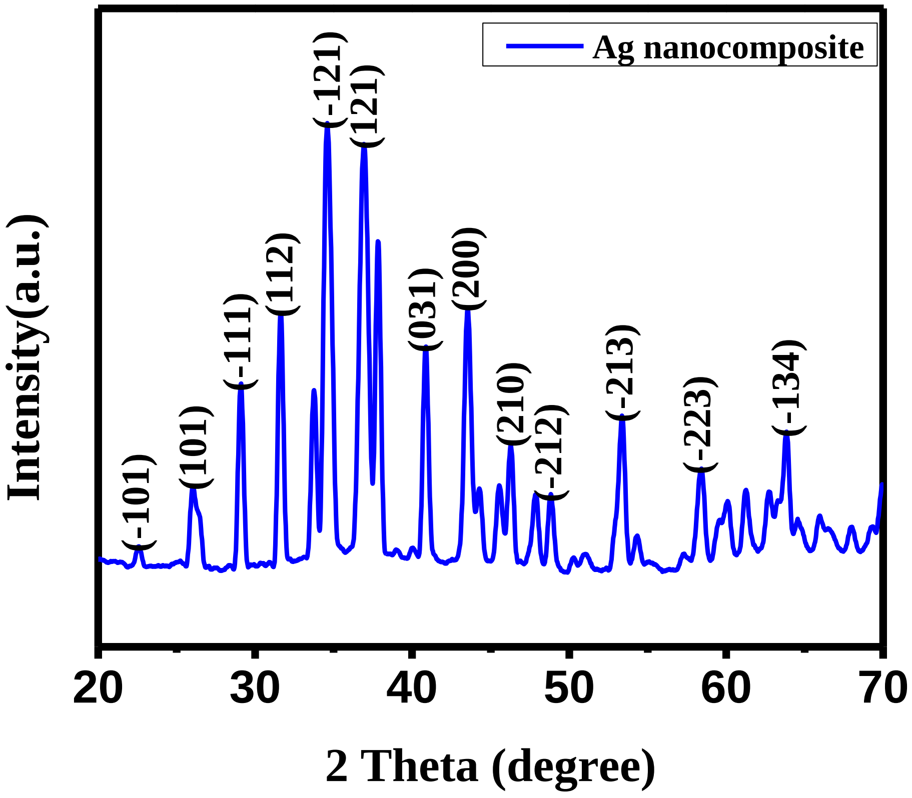

Fig.46. PXRD pattern of Ag nanocomposite derived by L-Cysteine

II. L-Cysteine CD with $AgNO_3$ at 100°C (Ag nanocomposite)

The peaks at 22.5°, 26°, 29°, 31.7^{o}, 34.5^{o}, 36.9^{o}, 40.8^{o}, 43.5^{o}, 45.4^{o}, 48.6^{o}, 53.3^{o}, 58.3^{o}, and 63.9^{o} corresponding to (-101), (111), (121), (031), (200), (210), (212), (-213), (-223), and (-134) Bragg reflections, respectively, show that the silver nanocomposite formed. The silver nanocomposite generated by employing L-Cysteine are crystalline in nature, according to X-ray diffraction data. The literature corroborated this information.[14]

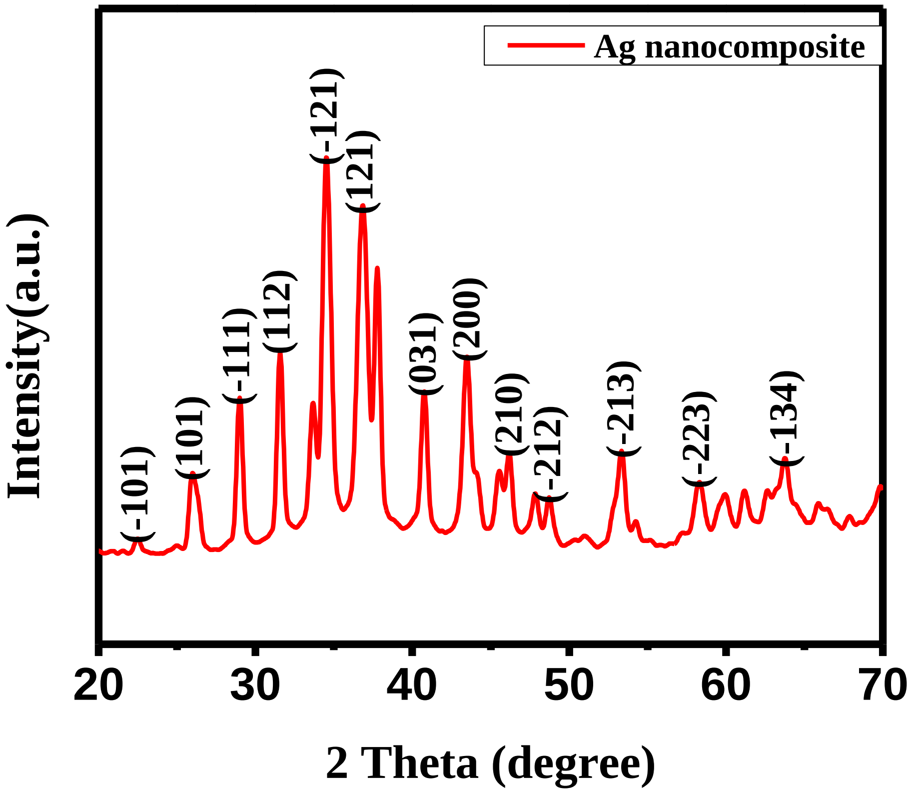

Fig.47. PXRD pattern of Ag nanocomposite derived by L-Cysteine CD

III. L-Cysteine + Citric acid with $AgNO_3$ at 200°C (Ag nanocomposite)

The peaks at 22.5°, 26°, 29°, 31.7^{o}, 34.5^{o}, 36.9^{o}, 40.8^{o}, 43.5^{o}, 45.4^{o}, 48.6^{o}, 53.3^{o}, 58.3^{o}, and 63.9^{o} corresponding to (-101), (111), (121), (031), (200), (210), (212), (-213), (-223), and (-134) Bragg reflections, respectively, show that the silver nanocomposite formed. The silver nanocomposite generated by employing L-Cysteine are crystalline in nature, according to X-ray diffraction data. The literature corroborated this information.[14]

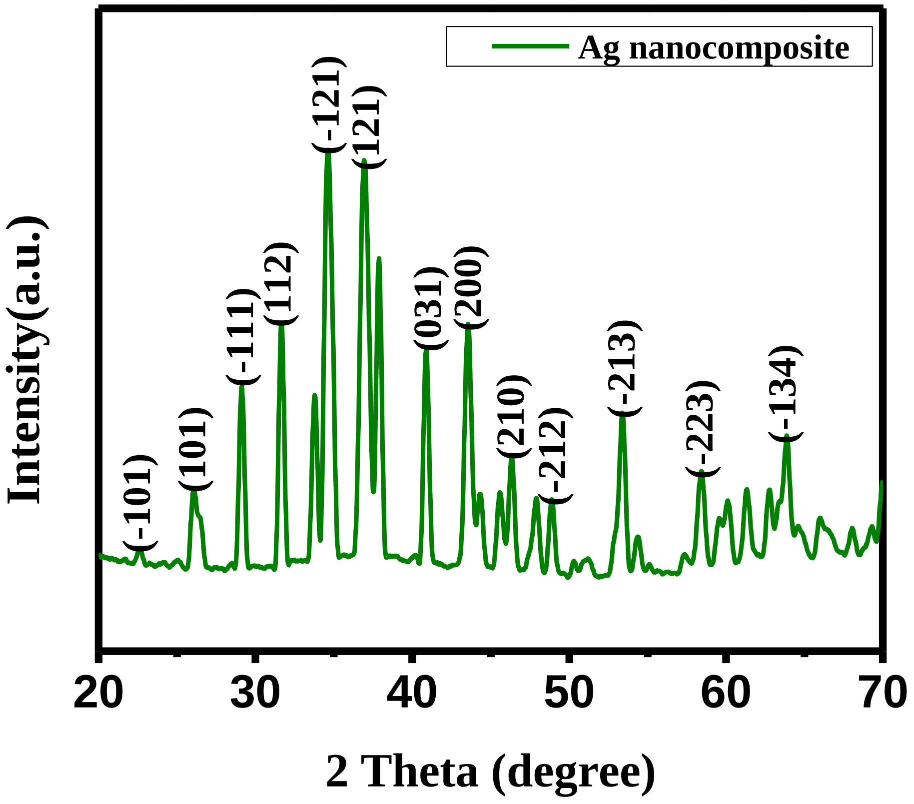

Fig.48. PXRD pattern of Ag nanocomposite derived by L-Cysteine + CA

5. Zeta Potential Measurements

Fig.49 shows the zeta potential measurements of the as synthesized silver nanoparticles. Zeta potential of citrate capped Ag NPs was found at -27.02 mv and PVP capped Ag NPs was found at -8.6 mv. The data shows that the citrate capped Ag NPs have high negative value and it is stable for several months. PVP capped Ag NPs have less stability compared to citrate capped Ag NPs due to less negative value of zeta potential.

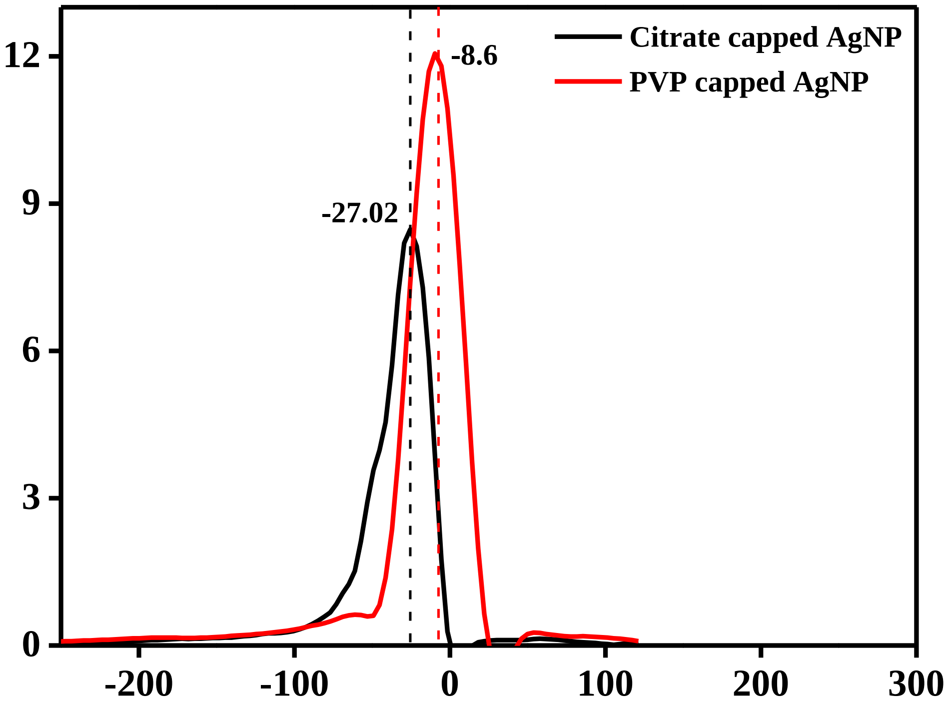

Fig.49. zeta potential of citrate capped Ag NPs and PVP capped Ag NPs

D. REACTION SCHEMES

Catalyst: 1) Citrate capped Ag NPs

2) PVP capped Ag NPs

3) Ag doped CD

hv = White light

Scheme 1 [12]

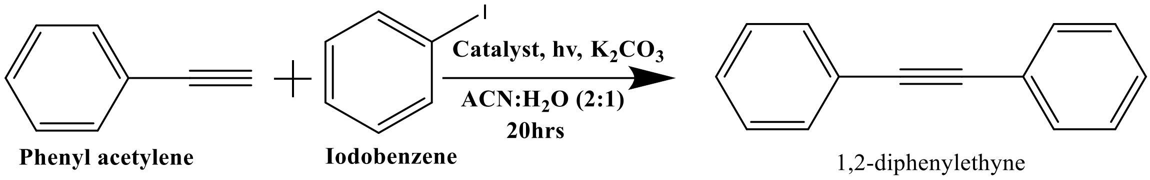

No Conversion

Scheme 2 [12]

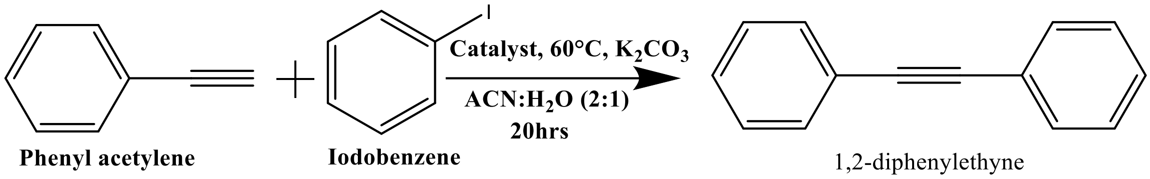

No Conversion

Scheme 3 [12]

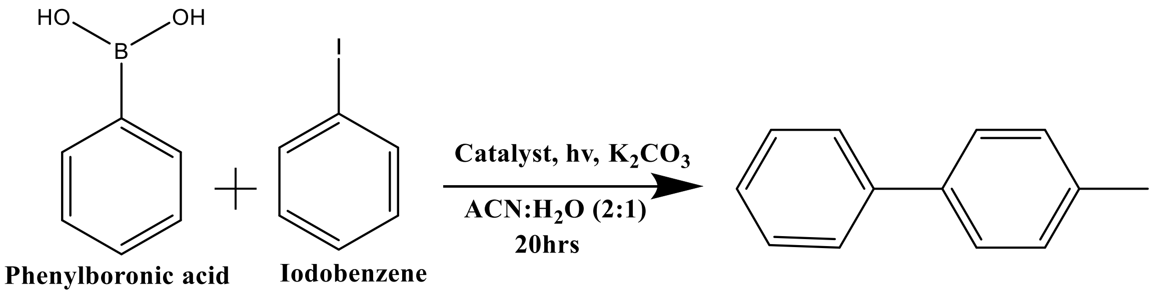

No Conversion

Scheme 4 [10]

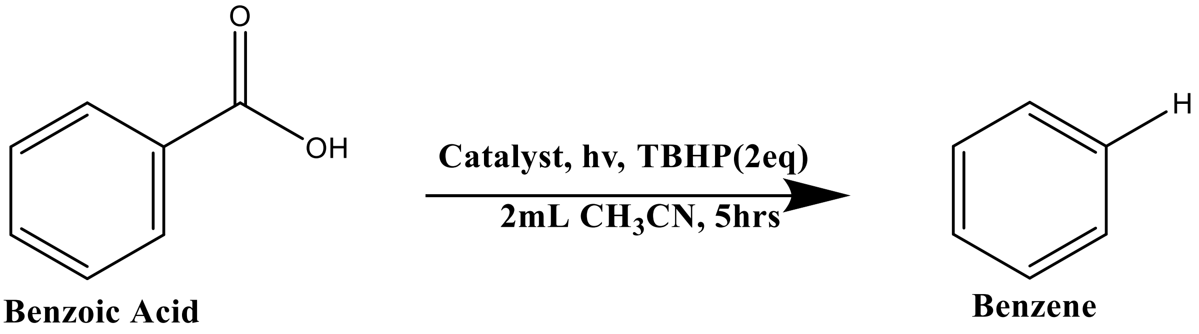

No Conversion

E. CONCLUSION

In summary, utilising sodium borohydride as a reducing agent, we successfully synthesised Ag NPs capped with sodium citrate and Polyvinyl pyrrolidone (PVP) using a straightforward chemical reduction process. Synthesized Ag NPs were characterised using a variety of techniques, including FTIR, SEM, PXRD, and UV–Vis. It was discovered that by managing the number of NPs injected, the average particle size may be controlled with a narrow size distribution. The synthesised NPs were shown to be stable for two months after preparation, indicating that they can be used for a long time. The generated size-controlled, well-dispersed Ag NPs may be dispersed in water and have prospective uses in dielectric and biological sectors. The use of silver nitrate, citric acid, and polyethyleneimine as raw materials to make water soluble, Ag doped, blue light emitting CDs in a one-step method. Multiple characterization of our formed Ag doped CD were employed such as SEM, PXRD, UV-Vis, and fluorescence to characterize it. We have also tried some reactions mentioned in the report from our synthesized Ag NPs and Ag doped CD.

In the earlier reactions, the nanoparticles that were formed were derived from the reported literature. Post making some amends in this project, we experimented with the thought to create nanoparticles that may function as better photocatalysts than their predecessors. Keeping that in mind, we were able to synthesize Ag nanocomposite successfully through the L-Cysteine, L-Cysteine Carbon dot and the mixture of L-Cysteine and Citric Acid. These synthesized Ag Nanocomposite were characterised using a variety of techniques, including FT-IR, SEM, PXRD, and UV–Vis. The resultant Carbon dot (supernatant) formed in the reaction was studied through UV-Vis and fluorescence Spectrum. In all the characterisations observed so far, we may conclude that the synthesised Ag Nanocomposite might work as a potential photocatalyst.

F. REFERENCES

1. P. Prinsen, R. Luque, Introduction to Nanocatalysts, *Nanoparticle Design and Characterisation for Catalytic Application in Sustainable Chemistry*, **2019**, *1*.
2. R. K. Sharma, S. Yadav, S. Dutta, H. B. Kale, I. R. Warkad, R. Zboril, R. S. Varma and M. B. Gawande, *Chem. Soc. Rev.*, **2021**,*50*, 11293-11380.
3. D. Zhao, X. Liu, R. Zhang, X. Xiao, J. Li D, *Zhao et al. J. Inorg. Biochem.*, **2021**,*214*,111306.
4. C.Y. Flores, C. Diaz a, A. Rubert, G.A. Benítez, M.S. Moreno, M.A. Fernández Lorenzo de Mele, R.C. Salvarezza, P.L. Schilardi, C. Vericat, C.Y. Flores et al. *J. Colloid Interface Sci.*, **2010**, *350*, 402–408.
5. A. Mirzaei, K. Janghorban, B. Hashemi, M. Bonyani, S. G. Leonardi, Giovanni Neri, *J. Nanostruct. Chem.*, **2017**, *7*, 37–46.
6. M. Kumar, P. Devi, A. Kumar, *J Mater Sci: Mater Electron*, **2017**, *28*, 5014–5020.
7. B. Ajitha, Y. Ashok Kumar Reddy, P. Sreedhara Reddy, Hwan-Jin Jeon and Chi Won Ahn, *RSC Adv*., **2016,** *6*, 36171–36179.
8. A. J. Kora and L. Rastogi, **2013**, *10.1155*, 871097.
9. Mohammed J. Haider, Mohammed S. Mehdi, *Int. j. sci. eng.*, *5*, 7, **2014**, ISSN 2229-5518.
10. Kun Zhan and Yi Li, *Catalysts*, **2017**, *7*, 314.
11. V. K. Rao and T. Radhakrishnan, *J. Mater. Chem. A*, **2013**, *1*, 13612–13618.
12. P. Venkatesan and J. Santhanalakshmi, *Langmuir*, **2010**, *26*, 12225–12229.
13. M. Palencia, A. Cordoba, Bernabe L. Rivas**,** *Colloid Polym. Sci.*, **2014**, *292*, 619–626.
14. Akl M. Awwad, Nidá M. Salem, Marwa M. Aqarbeh and Fatin M. Abdulaziz, *Chem. In*, **2020**, *6*, 42-48.
15. *Phys. Chem. Chem. Phys*., **2014**, *16*, 1788-1797.
16. *Junjun Liu, Rui Li, and Bai Yang, ACS Cent*. Sci., **2020**, *6*, *12*, 2179-2195.